Iranian Journal of Numerical Analysis and Optimization
Vol. 16, No. 4, 2026, pp 1189–1229
https://doi.org/10.22067/ijnao.2026.97711.1835
https://ijnao.um.ac.ir/

Research Article

Fractional order Chelyshkov wavelet for solving variable coefficients Caputo time-fractional convection-diffusion equation

S. Sabir* and A. Ahmad

Abstract

Convection-diffusion equations are widely used to describe transport processes and arise in numerous scientific and engineering applications, including heat transfer, contaminant transport in porous media, groundwater flow, chemical reactions, and biological systems. However, many real-world transport phenomena exhibit memory properties that classical convection-diffusion equations cannot adequately represent. To address such nonlocal temporal effects, time-fractional convection-diffusion equations have been introduced, in which fractional derivatives provide a realistic description of anomalous diffusion. This work proposes a novel wavelet-based numerical method for solving a variable-coefficient Caputo time-fractional convection-diffusion equation using fractional-order Chelyshkov wavelets. The method constructs fractional Chelyshkov wavelets from fractional Chelyshkov polynomials and derives corresponding fractional operational matrices. The proposed wavelet basis functions, together with an operational matrix formulation, transform the time-fractional convection-diffusion equation into a

*Corresponding author

Received 5 February 2026; revised 19 June 2026; accepted 25 July 2026

Sufia Sabir
Department of Mathematics and Computing Technology, National Institute of Technology Patna, Patna, 800005, Bihar, India. e-mail: sufias.phd22.ma@nitp.ac.in

Ayaz Ahmad
Department of Mathematics and Computing Technology, National Institute of Technology Patna, Patna, 800005, Bihar, India. e-mail: ayaz@nitp.ac.in

How to cite this article
Sabir, S. and Ahmad, A., Fractional order Chelyshkov wavelet for solving variable coefficients Caputo time-fractional convection-diffusion equation. *Iran. J. Numer. Anal. Optim.*, 2026; 16(4): 1189-1229. https://doi.org/10.22067/ijnao.2026.97711.1835

system of algebraic equations. The stability, convergence, and error estimates are established. To demonstrate the effectiveness and precision of the proposed method, several numerical examples are provided. CPU time and memory usage are reported for different numbers of basis functions. The numerical results indicate that the fractional Chelyshkov wavelets provide an efficient representation of smooth solutions, achieving high accuracy with a relatively small number of basis functions.

AMS subject classifications (2020): 35A01, 65L10, 65L12, 65L20, 65L70.

Keywords: Caputo time fractional convection-diffusion equation; Fractional Chelyshkov wavelet; Operational matrix; Stability; Convergence and error analysis.

1 Introduction

In recent years, models of fractional-order partial differential equations have been developed and studied across many research areas, including finance, fluid mechanics, plasma physics, biology, mechanics of materials, and chemistry. One of the most significant examples of a fractional partial differential equation is the convection-diffusion equation. Many physical phenomena, such as oil reservoir models, particle motion, heat transfer, global weather, energy transfer, and mass transfer, can be explained by the convection-diffusion equation. However, the classical convection–diffusion equation is often inadequate for describing anomalous diffusion phenomena arising from heterogeneous media or complex particle transport mechanisms encountered in natural systems. To tackle this situation, fractional convection-diffusion equations have been introduced. The classification of fractional partial differential equations includes space and time fractional, space fractional, and time fractional. In this article, we have considered the time fractional convection-diffusion equation (TFCDE) with a variable coefficient given as

$$\frac{\partial^\gamma \mathcal{U}(s,t)}{\partial t^\gamma} + a(s)\frac{\partial \mathcal{U}(s,t)}{\partial s} + b(s)\frac{\partial^2 \mathcal{U}(s,t)}{\partial s^2} = f(s,t)$$

with the initial condition (I.C) and boundary conditions (B.Cs)

$$\mathcal{U}(s,0) = q(s), \qquad \mathcal{U}(0,t) = f_0(t), \qquad \mathcal{U}(1,t) = f_1(t),$$

where $a(s)$ and $b(s) \neq 0$ are smooth functions, q, f_0, and $f_1 \in L^2[0,1)$, and $f(\cdot,\cdot)$ is a function in $L^2([0,1) \times [0,1))$.

Analytical solutions to fractional partial differential equations are not possible in many cases. So, developing stable, high-precision numerical methods has become a major focus of research. Various numerical methods, including the variational iteration method [39, 6], the finite element method [13], the finite difference method [34, 9], the operational method [14], the Ritz approximation method [15], the Tau method [1, 23], and so on, are used to solve fractional partial differential equations. To address the fractional convection-diffusion equation, several numerical techniques have been used, such as the discontinuous Galerkin method [25], the Sinc-Legendre collocation method [24], the Gegenbauer method [8], the Haar wavelet method [3], the Sinc and B-spline scaling functions [2], radial basis functions [35], the Chebyshev collocation method [41], and the Fibonacci wavelet method [38]. Wavelet-based numerical methods are highly effective for solving various classes of fractional partial differential equations due to their low complexity, rapid convergence, and reasonable computational efficiency. Wavelets are a family of functions that are obtained from the translation and dilatation of a single function called the "mother wavelet" [4]. A variety of wavelet and spectral-based methods, including Haar wavelet [40, 18], Bernoulli wavelet [21], Legendre wavelet [37, 29], Chebyshev wavelet [11], Hermite wavelet [5], Euler wavelet [36, 30, 28], Fibonacci wavelet [12], and B-spline wavelet [10] have been developed for fractional partial differential equations. Recently, Singh et al. [27, 31, 33, 32] proposed fractional wavelet operational matrix methods for different classes of fractional differential equations, demonstrating the effectiveness of wavelet approximations in reducing complex fractional models to algebraic systems. Motivated by the above work, we have proposed wavelet-based method for solving TFCDE with variable coefficients. We have found that most existing studies either focus on constant coefficients or use basis functions that do not specifically incorporate fractional characteristics. Additionally, a common characteristic of these existing methods is their reliance on high-resolution parameters to achieve high-precision results. When dealing with fractional equations, increasing the resolution parameter leads to a computational cost that grows exponentially due to the nonlocal nature of fractional derivatives, matrix ill-conditioning, which degrades stability during computation, and severe round-off error propagation.

Novelty and main contribution of this work:

To overcome the above limitations, this work introduces novel fractional Chelyshkov wavelets (FCW) and an operational matrix framework for the numerical solution of the variable-coefficient TFCDE. The fractional structure of basis functions enables an efficient representation of solution behavior associated with memory effects. FCW can demonstrate signals at different levels of resolution due to its compact support. Our proposed method introduces several advantages over the existing literature:

- **Fractional basis framework:** Most of the studies for TFCDE with variable coefficients rely on classical polynomials, scaling functions, or nonfractional wavelet bases [38, 41, 2, 7, 24, 26]. The nonfractional wavelet basis cannot accurately approximate the fractional power terms present in some fractional differential equations. Also, the fractional derivatives of nonfractional wavelet bases cannot be represented exactly within the same basis space, so a large number of basis functions is required to approximate fractional-order terms. In contrast, the proposed method employs fractional basis functions to obtain the corresponding operational matrix, thereby providing a more natural representation of fractional operators.

- **Superior accuracy at low resolutions:** The FCW yields a strictly orthogonal basis, minimizing theoretical complexity while optimizing numerical efficiency. These basis functions match fractional physics and reduce truncation errors with very few terms.

- **Computation sparsity:** The algebraic system obtained by combining compact wavelet support and strict orthogonality is highly structured and sparse, reducing memory requirements during computer implementation and ensuring lower computational time.

The present article is organized as follows: The introduction is presented in section 1. Section 2 presents the fundamental definitions and properties. Fractional order Chelyshkov wavelets are presented in section 3. Approximation of a function using fractional Chelyshkov wavelets is explained in section 4. Fractional operational matrices of FCW are obtained in Section 5. Section 6 presents a description of a numerical method to solve fractional convection-diffusion. Section 7 presents the stability analysis of the proposed method. Convergence analysis is discussed in Section 8. Section 9 presents the error analysis of the proposed method. Numerical examples are presented in section 10 to demonstrate the precision and effectiveness of the proposed method. Section 11 presents the conclusion of the paper.

2 Preliminaries

This section provides some fundamental definitions and properties of fractional integrals and derivatives.

Definition 1. A real function $\mathcal{U}(s)$, $s > 0$, is said to be in space C_σ, $\sigma \in \mathbb{R}$, if there is a real number η ($\eta > \sigma$) such that $\mathcal{U}(s) = s^\eta \mathcal{U}_0(s)$, where $\mathcal{U}_0(s) \in C[0,\infty)$ and $\mathcal{U}(s) \in C_\sigma^n$ if $\mathcal{U}^n(s) \in C_\sigma$, $n \in \mathbb{N}$ [16].

Definition 2. The Riemann–Liouville fractional integral operator of order $\alpha \geq 0$ of a function $\mathcal{U}(s) \in C_\sigma, \sigma \geq -1$ is defined as [20]

$$ {}_0^{RL}I_t^\alpha \mathcal{U}(t) = \frac{1}{\Gamma(\alpha)} \int_0^t (t-z)^{\alpha-1} \mathcal{U}(z) dz. \tag{1} $$

Definition 3. The Caputo fractional derivative operator of order α is defined as [20]

$$ {}_0^{C}D_t^\alpha \mathcal{U}(t) = \frac{1}{\Gamma(n-\alpha)} \int_0^t (t-z)^{n-\alpha-1} \mathcal{U}^n(z) dz, \qquad n-1 < \alpha \leq n, \tag{2} $$

where $n \in \mathbb{N}, t > 0$ and $\mathcal{U} \in C_{-1}^n$.

Proposition 1. The following properties are satisfied by the Riemann–Liouville fractional integrals and Caputo fractional derivatives [20]

- ${}_0^{C}D_t^\alpha {}_0^{RL}I_t^\alpha \mathcal{U}(t) = \mathcal{U}(t)$,
- ${}_0^{RL}I_t^\alpha {}_0^{C}D_t^\alpha \mathcal{U}(t) = \mathcal{U}(t) - \sum_{k=0}^{n-1} \mathcal{U}^k(0^+) \frac{t^k}{k!}$,

where $n-1 < \alpha \leq n$.

3 Fractional order Chelyshkov wavelet

Fractional Chelyshkov wavelets [17] are presented in this section. The definition of the Chelyshkov wavelet is

$$ \psi_{n,m}(t) = \begin{cases} 2^{\frac{k-1}{2}} \sqrt{2m+1} \rho_{m,M}(2^{k-1}t - n + 1), & \frac{n-1}{2^{k-1}} \leq t < \frac{n}{2^{k-1}}, \\ 0, & \text{otherwise.} \end{cases} \tag{3} $$

By applying the transformation $t = s^\beta$ in (3), we obtain the fractional Chelyshkov wavelet as

$$ \psi_{n,m}^\beta(s) = \begin{cases} 2^{\frac{k-1}{2}} \sqrt{2m+1} \rho_{m,M}(2^{k-1}s^\beta - n + 1), & (\frac{n-1}{2^{k-1}})^{\frac{1}{\beta}} \leq s < (\frac{n}{2^{k-1}})^{\frac{1}{\beta}}, \\ 0, & \text{otherwise,} \end{cases} \tag{4} $$

where $\beta \in \mathbb{R}^+, M \in \mathbb{Z}^+, k \in \mathbb{N}, n = 1, 2, \ldots, 2^{k-1}$ and $\rho_{m,M}$ denotes the Chelyshkov polynomial, which is given as

$$\rho_{m,M}(s) = \sum_{l=0}^{M-m-1} c_{l,m} s^{m+l}, \qquad m = 0, 1, \dots, M-1, \tag{5}$$

where $c_{l,m} = (-1)^l \binom{M-1-m}{l}\binom{M+m+l}{M-1-m}$.

For $k = 2, M = 2, \beta = 0.5$, the four basis functions are given as

$$\psi_{1,0}^{0.5}(s) = \begin{cases} -0.707107(-1+3(-1+4s^{0.5})), & 0 \le s < 0.25, \\ 0, & \text{otherwise}, \end{cases}$$

$$\psi_{1,1}^{0.5}(s) = \begin{cases} 4.89898 s^{0.5}, & 0 \le s < 0.25, \\ 0, & \text{otherwise}, \end{cases}$$

$$\psi_{2,0}^{0.5}(s) = \begin{cases} -0.707107(-1+3(-3+4s^{0.5})), & 0.25 \le s < 1, \\ 0, & \text{otherwise}, \end{cases}$$

$$\psi_{2,1}^{0.5}(s) = \begin{cases} 2.44948(-1+2s^{0.5}), & 0.25 \le s < 1, \\ 0, & \text{otherwise}. \end{cases}$$

The fractional Chelyshkov wavelets in two dimensions are given as

$$\psi_{n_1,m_1,n_2,m_2}^{\alpha,\beta}(s,t) = \begin{cases} 2^{\frac{k_1-1}{2}} 2^{\frac{k_2-1}{2}} \sqrt{2m_1+1}\sqrt{2m_2+1} & \text{if } \left(\frac{n_1-1}{2^{k_1-1}}\right)^{\frac{1}{\alpha}} \le s < \left(\frac{n_1}{2^{k_1-1}}\right)^{\frac{1}{\alpha}}, \\ \times \rho_{m_1,M_1}(2^{k_1-1}s^\alpha - n_1 + 1) & \left(\frac{n_2-1}{2^{k_2-1}}\right)^{\frac{1}{\beta}} \le t < \left(\frac{n}{2^{k_2-1}}\right)^{\frac{1}{\beta}}, \\ \times \rho_{m_2,M_2}(2^{k_2-1}t^\beta - n_2 + 1), & \\ 0, & \text{otherwise}. \end{cases}$$

Lemma 1. The orthonormal property of $\psi_{n_1,m_1,n_2,m_2}^{\alpha,\beta}(s,t)$ on $[0,1) \times [0,1)$ with respect to the weight function $w_{\alpha,\beta}(s,t) = \alpha\beta s^{\alpha-1}t^{\beta-1}$ is considered as follows:

$$\int_0^1 \int_0^1 w_{\alpha,\beta}(s,t)\psi_{n_1,m_1,n_2,m_2}^{\alpha,\beta}(s,t)\psi_{n_1',m_1',n_2',m_2'}^{\alpha,\beta}(s,t)dsdt$$
$$= \delta_{n_1,n_1'}\delta_{m_1,m_1'}\delta_{n_2,n_2'}\delta_{m_2,m_2'}.$$

Proof. Due to the orthonormal property of FCW, we have

$$\int_0^1 w_\alpha(t)\psi^\alpha_{n_1,m_1}(t)\psi^\alpha_{n_2,m_2}(t)dt = \delta_{n_1,n_2}\delta_{m_1,m_2}. \tag{6}$$

Now,

$$\begin{aligned}
&\int_0^1\int_0^1 w_{\alpha,\beta}(s,t)\psi^{\alpha,\beta}_{n_1,m_1,n_2,m_2}(s,t)\psi^{\alpha,\beta}_{n_1',m_1',n_2',m_2'}(s,t)dsdt\\
&=\int_0^1\int_0^1 \alpha\beta s^{\alpha-1}t^{\beta-1}\psi^\alpha_{n_1,m_1}(s)\psi^\beta_{n_2,m_2}(t)\psi^\alpha_{n_1',m_1'}(s)\psi^\beta_{n_2',m_2'}(t)dsdt\\
&=\int_0^1 \alpha s^{\alpha-1}\psi^\alpha_{n_1,m_1}(s)\psi^\alpha_{n_1',m_1'}(s)ds\int_0^1 \beta t^{\beta-1}\psi^\beta_{n_2,m_2}(t)\psi^\beta_{n_2',m_2'}(t)dt\\
&=\delta_{n_1,n_1'}\delta_{m_1,m_1'}\delta_{n_2,n_2'}\delta_{m_2,m_2'}.
\end{aligned}$$

□

4 Function approximation using FCW

A function $\mathcal{U}(s,t)\in L^2([0,1)\times[0,1))$ can be expanded in terms of FCW as

$$\mathcal{U}(s,t)=\sum_{n_1=1}^{2^{k_1-1}}\sum_{n_2=1}^{2^{k_2-1}}\sum_{m_1=0}^{\infty}\sum_{m_2=0}^{\infty} r_{n_1,n_2,m_1,m_2}\psi^\alpha_{n_1,m_1}(s)\psi^\beta_{n_2,m_2}(t), \tag{7}$$

where $r_{n_1,n_2,m_1,m_2}\in\mathbb{R}$. By truncating the power series to order M_1-1 in s and M_2-1 in t, we approximate $\mathcal{U}(s,t)$ as

$$\mathcal{U}(s,t)\approx\sum_{n_1=1}^{2^{k_1-1}}\sum_{n_2=1}^{2^{k_2-1}}\sum_{m_1=0}^{M_1-1}\sum_{m_2=0}^{M_2-1} r_{n_1,n_2,m_1,m_2}\psi^\alpha_{n_1,m_1}(s)\psi^\beta_{n_2,m_2}(t),$$

$$\mathcal{U}(s,t)\approx\mathcal{U}^{\alpha,\beta}_{k_1,k_2,M_1,M_2}=\Psi^\alpha_{k_1,M_1}(s)\cdot R\cdot\Psi^\beta_{k_2,M_2}(t), \tag{8}$$

where

$$\Psi^\beta_{k,M}=\left[\psi^\beta_{1,0},\ldots,\psi^\beta_{1,M-1},\psi^\beta_{2,0},\ldots,\psi^\beta_{2,M-1},\ldots,\psi^\beta_{2^{k-1},M-1}\right]^\top, \tag{9}$$

and R is a matrix of order $2^{k_1-1}M_1\times 2^{k_2-1}M_2$ composed of FCW coefficients

$$\begin{aligned} r_{n_1,n_2,m_1,m_2} &= \left\langle \mathcal{U}(s,t), \psi^{\alpha}_{n_1,m_1}(s)\psi^{\beta}_{n_2,m_2}(t) \right\rangle \\ &= \int_0^1 \int_0^1 w_{\alpha,\beta}(s,t)\mathcal{U}(s,t)\psi^{\alpha}_{n_1,m_1}(s)(\psi^{\beta}_{n_2,m_2}(t))^{\top} dsdt, \end{aligned}$$

$$1 \le n_1 \le 2^{k_1-1}, \qquad 0 \le m_1 \le M_1 - 1, 1 \le n_2 \le 2^{k_2-1}, \qquad 0 \le m_2 \le M_2 - 1.$$

The following collocation points are taken into account:

$$\begin{aligned} s_i &= \left(\frac{2i-1}{2^{k_1} M_1} \right)^{\frac{1}{\alpha}}, \qquad i = 1, 2, \ldots, 2^{k_1-1} M_1, \\ t_j &= \left(\frac{2j-1}{2^{k_2} M_2} \right)^{\frac{1}{\beta}}, \qquad j = 1, 2, \ldots, 2^{k_2-1} M_2. \end{aligned} \tag{10}$$

5 Riemann integration operational matrix of fractional Chelyshkov wavelet

Theorem 1. The Riemann integral of FCW vector $\Psi^{\beta}_{k,M}(s)$ can be approximated by fractional operational matrix S^{γ} which is given as

$$ {}_0^{RL}I_s^{\gamma}(\Psi^{\beta}_{k,M}(s)) \approx S^{\gamma}\Psi^{\beta}_{k,M}(s), \tag{11}$$

where S^{γ} is a square matrix of order $2^{k-1}M$ and the elements of the fractional integral of the FCW vector $\Psi^{\beta}_{k,M}(s)$ are as follows:

$$ {}_0^{RL}I_s^{\gamma}(\psi^{\beta}_{n,m}(s)) \approx \sum_{v=1}^{2^{k-1}} \sum_{l=0}^{M-1} \Lambda^{\gamma;nm}_{vl} \psi^{\beta}_{v,l}(s), \tag{12}$$

where

$$\Lambda^{\gamma;nm}_{vl} = \begin{cases} \xi_{mk} \sum_{j=0}^{M-m-1} (-1)^j \binom{M-1-m}{j} \binom{M+m+j}{M-1-m} 2^{(k-1)(m+j)} d^{1m}_{vl}, & n = 1, \\ \xi_{mk} \sum_{j=0}^{M-m-1} \sum_{p=0}^{m+j} (-1)^{m+2j-p} \binom{M-1-m}{j} \binom{M+m+j}{M-1-m} & \\ \qquad \times \binom{m+j}{p} (n-1)^{m+j-p} 2^{(k-1)p} d^{np}_{vl}, & n \neq 1, \end{cases}$$

and $\xi_{mk} = 2^{\frac{k-1}{2}}\sqrt{2m+1}$.

Proof. We obtain the fractional integration of FCW vector $\Psi^{\beta}_{k,M}(s)$, which is given as follows:

$$ {}_0^{RL}I_s^{\gamma}\Psi_{k,M}^{\beta}(s) \approx S^{\gamma}\Psi_{k,M}^{\beta}(s). $$

The expression in (4) can be rewritten as

$$ \psi_{n,m}^{\beta}(s) = 2^{\frac{k-1}{2}}\sqrt{2m+1}\rho_{m,M}(2^{k-1}s^{\beta}-n+1)\times\chi(s)\big|_{s\ \in[(\frac{n-1}{2^{k-1}})^{\frac{1}{\beta}},(\frac{n}{2^{k-1}})^{\frac{1}{\beta}})}. \tag{13} $$

Using the definition of Chelyshkov polynomial from (5), we have

$$ \begin{aligned} &\rho_{m,M}(2^{k-1}s^{\beta}-n+1) \\ &= \sum_{j=0}^{M-m-1}(-1)^j\binom{M-1-m}{j}\binom{M+m+j}{M-1-m}(2^{k-1}s^{\beta}-n+1)^{m+j}. \end{aligned} \tag{14} $$

Substituting (14) in (13), we get

$$ \begin{aligned} &\psi_{n,m}^{\beta}(s) \\ &= \xi_{mk}\sum_{j=0}^{M-m-1}(-1)^j\binom{M-1-m}{j}\binom{M+m+j}{M-1-m}(2^{k-1}s^{\beta}-n+1)^{m+j} \\ &\quad\times\chi(s)\big|_{s\ \in[(\frac{n-1}{2^{k-1}})^{\frac{1}{\beta}},(\frac{n}{2^{k-1}})^{\frac{1}{\beta}})}, \end{aligned} \tag{15} $$

where $\xi_{mk} = 2^{\frac{k-1}{2}}\sqrt{2m+1}$ and $\chi(s)$ is characteristic function given as

$$ \chi(s)\big|_{s\ \in[(\frac{n-1}{2^{k-1}})^{\frac{1}{\beta}},(\frac{n}{2^{k-1}})^{\frac{1}{\beta}})} = \begin{cases} 1, & s\in[(\frac{n-1}{2^{k-1}})^{\frac{1}{\beta}},(\frac{n}{2^{k-1}})^{\frac{1}{\beta}}), \\ 0, & \text{otherwise}. \end{cases} $$

Putting $n=1$ in (15),

$$ \begin{aligned} &\psi_{1,m}^{\beta}(s) \\ &= \xi_{mk}\sum_{j=0}^{M-m-1}(-1)^j\binom{M-1-m}{j}\binom{M+m+j}{M-1-m}(2^{k-1}s^{\beta})^{m+j} \\ &\quad\times\chi(s)\big|_{s\ \in[(\frac{n-1}{2^{k-1}})^{\frac{1}{\beta}},(\frac{n}{2^{k-1}})^{\frac{1}{\beta}})}. \end{aligned} \tag{16} $$

Taking the Riemann–Liouville integral on both sides of (16), we have

$$ {}_0^{RL}I_s^{\gamma}(\psi_{1,m}^{\beta}(s)) $$

$$= \xi_{mk} \sum_{j=0}^{M-m-1} (-1)^j \binom{M-1-m}{j} \binom{M+m+j}{M-1-m} 2^{(k-1)(m+j)}$$
$$\times {}_0^{RL}I_s^{\gamma} \left(s^{\beta(m+j)} \chi(s)\Big|_{s\ \in[(\frac{n-1}{2^{k-1}})^{\frac{1}{\beta}},(\frac{n}{2^{k-1}})^{\frac{1}{\beta}})} \right). \tag{17}$$

Now, with the help of the binomial expansion, we have

$$(2^{k-1}s^{\beta} - n + 1)^{m+j} = \sum_{p=0}^{m+j} \binom{m+j}{p} (2^{k-1}s^{\beta})^p (-1)^{m+j-p} (n-1)^{m+j-p}. \tag{18}$$

When $n = 2, 3, \ldots, 2^{k-1}$, using (18) in (15), we have

$$\psi_{n,m}^{\beta}(s)$$
$$= \xi_{mk} \sum_{j=0}^{M-m-1} (-1)^j \binom{M-1-m}{j} \binom{M+m+j}{M-1-m} \sum_{p=0}^{m+j} \binom{m+j}{p} (2^{k-1}s^{\beta})^p$$
$$\times (-1)^{m+j-p} (n-1)^{m+j-p} \times \chi(s)\Big|_{s\ \in[(\frac{n-1}{2^{k-1}})^{\frac{1}{\beta}},(\frac{n}{2^{k-1}})^{\frac{1}{\beta}})}. \tag{19}$$

Taking the Riemann–Liouville integral on both sides of (19), we have

$${}_0^{RL}I_s^{\gamma}(\psi_{n,m}^{\beta}(s))$$
$$= {}_0^{RL}I_s^{\gamma} \left(\xi_{mk} \sum_{j=0}^{M-m-1} (-1)^j \binom{M-1-m}{j} \binom{M+m+j}{M-1-m} \sum_{p=0}^{m+j} \binom{m+j}{p} \right.$$
$$\left. \times (2^{k-1}s^{\beta})^p (-1)^{m+j-p} (n-1)^{m+j-p} \times \chi(s)\Big|_{s\ \in[(\frac{n-1}{2^{k-1}})^{\frac{1}{\beta}},(\frac{n}{2^{k-1}})^{\frac{1}{\beta}})} \right),$$

$${}_0^{RL}I_s^{\gamma}(\psi_{n,m}^{\beta}(s))$$
$$= \xi_{mk} \sum_{j=0}^{M-m-1} (-1)^j \binom{M-1-m}{j} \binom{M+m+j}{M-1-m} \sum_{p=0}^{m+j} \binom{m+j}{p} 2^{(k-1)p}$$
$$\times (-1)^{m+j-p} (n-1)^{m+j-p} \times {}_0^{RL}I_s^{\gamma} \left(s^{\beta p} \chi(s)\Big|_{s\ \in[(\frac{n-1}{2^{k-1}})^{\frac{1}{\beta}},(\frac{n}{2^{k-1}})^{\frac{1}{\beta}})} \right). \tag{20}$$

We approximate ${}_0^{RL}I_s^{\gamma} \left(s^{\beta p} \chi(s)\Big|_{s\ \in[(\frac{n-1}{2^{k-1}})^{\frac{1}{\beta}},(\frac{n}{2^{k-1}})^{\frac{1}{\beta}})} \right)$ by $2^{k-1}M$ terms of FCW, we have

$${}_0^{RL}I_s^{\gamma} \left(s^{\beta p} \chi(s)\Big|_{s\ \in[(\frac{n-1}{2^{k-1}})^{\frac{1}{\beta}},(\frac{n}{2^{k-1}})^{\frac{1}{\beta}})} \right)$$

$$= h_{np}(s) \approx \sum_{v=1}^{2^{k-1}} \sum_{l=0}^{M-1} d_{vl}^{np} \psi_{v,l}^{\beta}(s) = D_{vl}^{\top} \Psi_{k,M}^{\beta}(s), \tag{21}$$

where $h_{np}(s) = \frac{1}{\Gamma(\gamma)} \int_0^s (s-z)^{\gamma-1} z^{\beta p} \chi(z)\big|_{z\ \in[(\frac{n-1}{2^{k-1}})^{\frac{1}{\beta}},(\frac{n}{2^{k-1}})^{\frac{1}{\beta}})} dz$,
and $D_{vl}^{\top} =< h_{np}(s), \Psi_{k,M}^{\beta}(s) >$. Substituting (21) in (17) and (20) gives

$$\begin{aligned}
&{}_0^{RL}I_s^{\gamma}(\psi_{1,m}^{\beta}(s)) \\
&\approx \xi_{mk} \sum_{j=0}^{M-m-1} (-1)^j \binom{M-1-m}{j} \binom{M+m+j}{M-1-m} 2^{(k-1)(m+j)} \\
&\quad \times \sum_{v=1}^{2^{k-1}} \sum_{l=0}^{M-1} d_{vl}^{1m} \psi_{v,l}^{\beta}(s) \\
&= \sum_{v=1}^{2^{k-1}} \sum_{l=0}^{M-1} \Lambda_{vl}^{\gamma;1m} \psi_{v,l}^{\beta}(s),
\end{aligned}$$

and

$$\begin{aligned}
&{}_0^{RL}I_s^{\gamma}(\psi_{n,m}^{\beta}(s)) \\
&\approx \xi_{mk} \sum_{j=0}^{M-m-1} \sum_{p=0}^{m+j} (-1)^{m+2j-p} \binom{M-1-m}{j} \binom{M+m+j}{M-1-m} \binom{m+j}{p} \\
&\quad \times 2^{(k-1)p} (n-1)^{m+j-p} \sum_{v=1}^{2^{k-1}} \sum_{l=0}^{M-1} d_{vl}^{np} \psi_{v,l}^{\beta}(s) \\
&= \sum_{v=1}^{2^{k-1}} \sum_{l=0}^{M-1} \Lambda_{vl}^{\gamma;nm} \psi_{v,l}^{\beta}(s),
\end{aligned}$$

where

$$\Lambda_{vl}^{\gamma;nm} = \begin{cases} \xi_{mk} \sum_{j=0}^{M-m-1} (-1)^j \binom{M-1-m}{j} \binom{M+m+j}{M-1-m} 2^{(k-1)(m+j)} d_{vl}^{1m}, & n = 1, \\ \xi_{mk} \sum_{j=0}^{M-m-1} \sum_{p=0}^{m+j} (-1)^{m+2j-p} \binom{M-1-m}{j} \binom{M+m+j}{M-1-m} & \\ \qquad \times \binom{m+j}{p} (n-1)^{m+j-p} 2^{(k-1)p} d_{vl}^{np}, & n \neq 1. \end{cases}$$

Thus

$${}_0^{RL}I_s^{\gamma}(\Psi_{k,M}^{\beta}(s)) \approx \sum_{v=1}^{2^{k-1}} \sum_{l=0}^{M-1} \Lambda_{vl}^{\gamma;nm} \psi_{v,l}^{\beta}(s) = S^{\gamma} \Psi_{k,M}^{\beta}(s),$$

$$S^{\gamma} = \begin{bmatrix} \Lambda_{10}^{\gamma;10} & \cdots & \Lambda_{1M-1}^{\gamma;10} & \cdots & \Lambda_{2^{k-1}0}^{\gamma;10} & \cdots & \Lambda_{2^{k-1}M-1}^{\gamma;10} \\ \Lambda_{10}^{\gamma;11} & \cdots & \Lambda_{1M-1}^{\gamma;11} & \cdots & \Lambda_{2^{k-1}0}^{\gamma;11} & \cdots & \Lambda_{2^{k-1}M-1}^{\gamma;11} \\ \vdots & \cdots & \vdots & \cdots & \vdots & \ddots & \vdots \\ \Lambda_{10}^{\gamma;\,2^{k-1}M-1} & \cdots & \Lambda_{1M-1}^{\gamma;\,2^{k-1}M-1} & \cdots & \Lambda_{2^{k-1}0}^{\gamma;\,2^{k-1}M-1} & \cdots & \Lambda_{2^{k-1}M-1}^{\gamma;\,2^{k-1}M-1} \end{bmatrix}.$$

The FCW operational matrix for $k = 2, M = 3, \beta = 1$, and $\gamma = 0.7$ is given as

$$S^{0.7} = \begin{bmatrix} 0.101545 & 0.1832 & 0.110702 & 0.0577836 & 0.0869881 & 0.100422 \\ -0.0414831 & 0.191149 & 0.312073 & 0.0856382 & 0.150711 & 0.179004 \\ 0.00760829 & -0.0286796 & 0.248597 & 0.189728 & 0.254836 & 0.268119 \\ 0 & 0 & 0 & 0.101545 & 0.1832 & 0.110702 \\ 0 & 0 & 0 & -0.0414831 & 0.191149 & 0.312073 \\ 0 & 0 & 0 & 0.00760829 & -0.0286796 & 0.248597 \end{bmatrix}.$$

□

6 The numerical method

In this section, we have considered the TFCDE with a variable coefficient

$$\frac{\partial^{\gamma}\mathcal{U}(s,t)}{\partial t^{\gamma}} + a(s)\frac{\partial \mathcal{U}(s,t)}{\partial s} + b(s)\frac{\partial^{2}\mathcal{U}(s,t)}{\partial s^{2}} = f(s,t), \tag{22}$$

with I.C and B.Cs

$$\mathcal{U}(s,0) = q(s), \tag{23}$$

$$\mathcal{U}(0,t) = f_0(t), \qquad \mathcal{U}(1,t) = f_1(t). \tag{24}$$

where $a(s)$, $b(s) \neq 0$ are smooth functions, q, f_0, and $f_1 \in L^2[0,1)$, and $f(\cdot,\cdot)$ is a function in $L^2([0,1)\times[0,1))$, with $\frac{\partial^{\gamma}\mathcal{U}(s,t)}{\partial t^{\gamma}} = {}_{0}^{C}D_t^{\gamma}\mathcal{U}(s,t)$.

To solve (22)–(23), we proceed as follows:

$$\frac{\partial^{2+\gamma}\mathcal{U}(s,t)}{\partial s^{2}\partial t^{\gamma}} \approx \Psi_{k_1,M_1}^{\alpha}(s)\cdot R\cdot \Psi_{k_2,M_2}^{\beta}(t), \tag{25}$$

where R is an unknown fractional Chelyshkov wavelet coefficient. We have

$$\int_0^s \Psi^{\alpha}_{k,M}(z)dz \approx S\Psi^{\alpha}_{k,M}(z), \tag{26}$$

where S denotes the integer-order integration operational matrix. Taking Riemann–Liouville fractional integral of order γ with respect to t on both sides of (25), we have

$$\begin{aligned}\frac{\partial^2\mathcal{U}(s,t)}{\partial s^2} &\approx \frac{\partial^2\mathcal{U}(s,t)}{\partial s^2}\Big|_{s=0} + \Psi^{\alpha}_{k_1,M_1}(s)R(S^{\gamma}\Psi^{\beta}_{k_2,M_2}(t))\\ &\approx q''(s) + \Psi^{\alpha}_{k_1,M_1}(s)R(S^{\gamma}\Psi^{\beta}_{k_2,M_2}(t)).\end{aligned} \tag{27}$$

Again, integrating twice with respect to s, we have

$$\begin{aligned}\mathcal{U}(s,t) \approx \mathcal{U}(0,t) &+ s\frac{\partial\mathcal{U}(s,t)}{\partial s}\Big|_{s=0} + q(s) - q(0) - sq'(0)\\ &+ (S^2\Psi^{\alpha}_{k_1,M_1}(s))^{\top}R(S^{\gamma}\Psi^{\beta}_{k_2,M_2}(t)).\end{aligned} \tag{28}$$

Putting $s = 1$ in (28), we have

$$\begin{aligned}\mathcal{U}(1,t) \approx &\mathcal{U}(0,t) + \frac{\partial\mathcal{U}(s,t)}{\partial s}\Big|_{s=0} + q(1) - q(0) - q'(0)\\ &+ (S^2\Psi^{\alpha}_{k_1,M_1}(1))^{\top}R(S^{\gamma}\Psi^{\beta}_{k_2,M_2}(t)),\end{aligned}$$

$$\begin{aligned}\frac{\partial\mathcal{U}(s,t)}{\partial s}\Big|_{s=0} \approx &- (S^2\Psi^{\alpha}_{k_1,M_1}(1))^{\top}R(S^{\gamma}\Psi^{\beta}_{k_2,M_2}(t)) + q(0)\\ &+ q'(0) - q(1) + f_1(t) - f_0(t)\\ =&J(t).\end{aligned}$$

Now (28) gives

$$\begin{aligned}\mathcal{U}(s,t) \approx &\mathcal{U}(0,t) + sJ(t) + q(s) - q(0) - sq'(0)\\ &+ (S^2\Psi^{\alpha}_{k_1,M_1}(s))^{\top}R(S^{\gamma}\Psi^{\beta}_{k_2,M_2}(t)).\end{aligned} \tag{29}$$

Taking the Caputo derivative with respect to t, we obtain

$$\begin{aligned}\frac{\partial^{\gamma}\mathcal{U}(s,t)}{\partial t^{\gamma}} \approx &- s(S^2\Psi^{\alpha}_{k_1,M_1}(1))^{\top}R(S^{\gamma}\Psi^{\beta}_{k_2,M_2}(t)) + s\frac{\partial^{\gamma}f_1(t)}{\partial t^{\gamma}} + (1-s)\frac{\partial^{\gamma}f_0(t)}{\partial t^{\gamma}}\\ &+ (S^2\Psi^{\alpha}_{k_1,M_1}(s))^{\top}R\Psi^{\beta}_{k_2,M_2}(t).\end{aligned} \tag{30}$$

Differentiating (29) with respect to s, we get

$$\frac{\partial \mathcal{U}(s,t)}{\partial s} \approx J(t) + q'(s) - q'(0) + (S\Psi^{\alpha}_{k_1,M_1}(s))^{\top} R(S^{\gamma}\Psi^{\beta}_{k_2,M_2}(t)). \tag{31}$$

Substituting (27), (30), and (31) into (22). The system of algebraic equations with the collocation points from (10) is obtained as

$$\begin{aligned}
&(S^2\Psi^{\alpha}_{k_1,M_1}(s))^{\top} R\Psi^{\beta}_{k_2,M_2}(t) - s(S^2\Psi^{\alpha}_{k_1,M_1}(1))^{\top} R(S^{\gamma}\Psi^{\beta}_{k_2,M_2}(t)) + s\frac{\partial^{\gamma} f_1(t)}{\partial t^{\gamma}} \\
&+ (1-s)\frac{\partial^{\gamma} f_0(t)}{\partial t^{\gamma}} + a(s)(J(t) + q'(s) - q'(0) \\
&+ (S\Psi^{\alpha}_{k_1,M_1}(s))^{\top} R(S^{\gamma}\Psi^{\beta}_{k_2,M_2}(t))) \\
&+ b(s)(q''(s) + \Psi^{\alpha}_{k_1,M_1}(s)R(S^{\gamma}\Psi^{\beta}_{k_2,M_2}(t))) = f(s,t).
\end{aligned} \tag{32}$$

We have solved the obtained system of equations using the LinearSolve command in Mathematica to obtain the value R. Finally, after putting the value of R in (28), we get the approximate solution.

7 Stability analysis

In this section, we present a perturbation analysis to study the stability of the proposed wavelet-based method. The system in (32) can be represented compactly in the following global matrix form

$$AC = F,$$

where A is the global operational matrix incorporating the matrix R along with the integer and fractional order operational matrix S, S^2, and S^{γ}, C represents the vector of unknown expansion coefficients, and F is the data vector containing the initial condition $q(s)$, boundary conditions $f_0(t), f_1(t)$, and the source term $f(s,t)$.

Next, we present the main stability theorem given as follows.

Theorem 2. Let $\mathcal{U}^{\alpha,\beta}_{k_1,k_2,M_1,M_2}(s,t)$ be the approximate solution obtained by applying the proposed method, and let $\mathcal{U}^{P;\alpha,\beta}_{k_1,k_2,M_1,M_2}(s,t)$ be the approximate solution obtained under perturbed conditions.

Case-1: If the perturbations occur only in the data vector F such that $A(C+\Delta C) = F + \Delta F$, and assuming the invertibility of A, then the stability error is bounded by

$$||\mathcal{U}^{\alpha,\beta}_{k_1,k_2,M_1,M_2}(s,t) - \mathcal{U}^{P;\alpha,\beta}_{k_1,k_2,M_1,M_2}(s,t)||$$

$$\leq |E(s,t)| + \Phi(s)\Phi(t)cond(A)\left(\frac{\|\Delta F\|}{\|F\|}\right)\|C\|.$$

Case-2: Let the perturbations simultaneously occur in both the global matrix A and the data vector F such that $(A+\Delta A)(C+\Delta C) = F + \Delta F$. Assuming the invertibility of A, and $cond(A)\left(\frac{\|\Delta A\|}{\|A\|}\right) < 1$, then the stability error is bounded by

$$\begin{aligned}
&||\mathcal{U}^{\alpha,\beta}_{k_1,k_2,M_1,M_2}(s,t) - \mathcal{U}^{P;\alpha,\beta}_{k_1,k_2,M_1,M_2}(s,t)|| \\
&\leq |E(s,t)| + \Phi(s)\Phi(t)\frac{cond(A)}{\left(1 - cond(A)\left(\frac{\|\Delta A\|}{\|A\|}\right)\right)} \\
&\quad\times\left[\frac{\|\Delta A\|}{\|A\|} + \frac{\|\Delta F\|}{\|F\|}\right]\|C\|,
\end{aligned}$$

where $\Phi(s) = \|(S^2\Psi^{\alpha}_{k_1,M_1}(s) - s(S^2\Psi^{\alpha}_{k_1,M_1}(1)))\|$, $\Phi(t) = \|S^{\gamma}\Psi^{\beta}_{k_2,M_2}(t)\|$, and $E(s,t) = |\Delta q(s)| + |(1-s)||\Delta f_0(t) - \Delta f_0(0)| + |s||\Delta f_1(t) - \Delta f_1(0)|$.

Proof. For the simplicity of notation, we denote $\mathcal{U}^{\alpha,\beta}_{k_1,k_2,M_1,M_2}(s,t) = u(s,t)$, and $\mathcal{U}^{P;\alpha,\beta}_{k_1,k_2,M_1,M_2}(s,t) = u^P(s,t)$. All matrix and vector norms reported in the proof are using infinity norms. From (29), we have the following representation for $u(s,t)$

$$\begin{aligned}
u(s,t) =& f_0(t) + q(s) - q(0) + s(q(0) - q(1) + f_1(t) - f_0(t)) \\
&+ (S^2\Psi^{\alpha}_{k_1,M_1}(s) - s(S^2\Psi^{\alpha}_{k_1,M_1}(1)))^{\top} R(S^{\gamma}\Psi^{\beta}_{k_2,M_2}(t)).
\end{aligned} \tag{33}$$

The perturbed solution $u^P(s,t)$ after introducing a small perturbation into the initial data $(q(s) \to q(s) + \Delta q(s))$, the boundary data $(f_0(t) \to \Delta f_0(t))$, $(f_1(t) \to f_1(t) + \Delta f_1(t))$, and solution vector $(R \to R + \Delta R)$, is given as

$$\begin{aligned}
u^P(s,t) =& (f_0(t) + \Delta f_0(t)) + (q(s) + \Delta q(s)) - (q(0) + \Delta q(0)) \\
&+ s((q(0) + \Delta q(0)) - (q(1) + \Delta q(1)) + (f_1(t) + \Delta f_1(t)) \\
&- (f_0(t) + \Delta f_0(t)) + (S^2\Psi^{\alpha}_{k_1,M_1}(s) \\
&- s(S^2\Psi^{\alpha}_{k_1,M_1}(1)))^{\top}(R + \Delta R)(S^{\gamma}\Psi^{\beta}_{k_2,M_2}(t)).
\end{aligned} \tag{34}$$

Subtracting (34) from (33), and taking the norm on both sides

$$\begin{aligned}
\|u(s,t) - u^P(s,t)\| =& \| - \Delta f_0(t) - \Delta q(s) + \Delta q(0) - s(\Delta q(0) - \Delta q(1) \\
&+ \Delta f_1(t) - \Delta f_0(t)) + (S^2\Psi^{\alpha}_{k_1,M_1}(s)
\end{aligned}$$

$$- s(S^2\Psi^{\alpha}_{k_1,M_1}(1)))^{\top}\Delta R(S^{\gamma}\Psi^{\beta}_{k_2,M_2}(t))\|. \tag{35}$$

Now, we apply the physical compatibility condition at the intersection corner of the domain, such that $\Delta q(0) = \Delta f_0(0)$ and $\Delta q(1) = \Delta f_1(0)$, we get

$$\begin{aligned} &\Delta f_0(t) + \Delta q(s) - \Delta q(0) + s(\Delta q(0) - \Delta q(1) + \Delta f_1(t) - \Delta f_0(t)) \\ &= \Delta f_0(t) + \Delta q(s) - \Delta f_0(0) + s(\Delta f_0(0) - \Delta f_1(0) + \Delta f_1(t) - \Delta f_0(t)). \end{aligned} \tag{36}$$

Substituting (36) in (35), we get

$$\begin{aligned} \|u(s,t) - u^P(s,t)\| \le{}& |\Delta q(s)| + |(1-s)||\Delta f_0(t) - \Delta f_0(0)| \\ &+ |s||\Delta f_1(t) - \Delta f_1(0)| \\ &+ \|(S^2\Psi^{\alpha}_{k_1,M_1}(s) - s(S^2\Psi^{\alpha}_{k_1,M_1}(1)))^{\top}\Delta R(S^{\gamma}\Psi^{\beta}_{k_2,M_2}(t))\|. \end{aligned} \tag{37}$$

Therefore

$$\begin{aligned} &\|u(s,t) - u^P(s,t)\| \\ &\le |E(s,t)| + \|(S^2\Psi^{\alpha}_{k_1,M_1}(s) - s(S^2\Psi^{\alpha}_{k_1,M_1}(1)))^{\top}\Delta R(S^{\gamma}\Psi^{\beta}_{k_2,M_2}(t))\|. \end{aligned} \tag{38}$$

Now, the Kronecker vectorization identity is given as

$$vec(X^{\top}YZ) = (Z^{\top} \otimes X^{\top})vec(Y), \tag{39}$$

where X, Y, and Z are any three matrices.

Using (39) in (38) and taking $\Delta C = vec(\Delta R)$, we have

$$\begin{aligned} &\|u(s,t) - u^P(s,t)\| \\ &\le |E(s,t)| + \|(S^{\gamma}\Psi^{\beta}_{k_2,M_2}(t))^{\top} \otimes (S^2\Psi^{\alpha}_{k_1,M_1}(s) - s(S^2\Psi^{\alpha}_{k_1,M_1}(1)))\|\|\Delta C\|. \end{aligned} \tag{40}$$

For any matrix X and Y, the Kronecker matrix splitting norm property gives

$$\|X \otimes Y\| = \|X\|\|Y\|.$$

Thus

$$\begin{aligned} &\|u(s,t) - u^P(s,t)\| \\ &\le |E(s,t)| + \|(S^2\Psi^{\alpha}_{k_1,M_1}(s) - s(S^2\Psi^{\alpha}_{k_1,M_1}(1)))\|\|S^{\gamma}\Psi^{\beta}_{k_2,M_2}(t)\|\|\Delta C\|. \end{aligned} \tag{41}$$

Let us define

$$\Phi(s) = \|(S^2\Psi^{\alpha}_{k_1,M_1}(s) - s(S^2\Psi^{\alpha}_{k_1,M_1}(1)))\|, \qquad \Phi(t) = \|S^{\gamma}\Psi^{\beta}_{k_2,M_2}(t)\|.$$

Therefore

$$\|u(s,t) - u^P(s,t)\| \leq |E(s,t)| + \Phi(s)\Phi(t)\|\Delta C\|. \tag{42}$$

Case 1: If the perturbation occurs only in the data vector F such that

$$A(C + \Delta C) = F + \Delta F. \tag{43}$$

Subtracting $AC = F$ from (43), we get

$$A\Delta C = \Delta F.$$

Using the invertibility of A gives

$$\Delta C = A^{-1}\Delta F.$$

Taking the norm of both sides, we get

$$\|\Delta C\| \leq \|A^{-1}\|\|\Delta F\|. \tag{44}$$

Also, from $AC = F$, we have

$$\frac{1}{\|C\|} \leq \frac{\|A\|}{\|F\|}. \tag{45}$$

From (44) and (45), we have

$$\|\Delta C\| \leq \|A\|\|A^{-1}\|\left(\frac{\|\Delta F\|}{\|F\|}\right)\|C\|. \tag{46}$$

For any nonsingular matrix A, the condition number is defined as

$$cond(A) = \|A\|\|A^{-1}\|.$$

For numerical computation, we take the ratio

$$p_1 = \frac{\|\Delta C\|}{cond(A)\|C\|}\left(\frac{\|F\|}{\|\Delta F\|}\right).$$

Value $p_1 \leq 1$ confirms that the theoretical stability bound is satisfied.

Substituting (46) in (42), we get

$$\|u(s,t) - u^P(s,t)\| \leq |E(s,t)| + \Phi(s)\Phi(t)cond(A)\left(\frac{\|\Delta F\|}{\|F\|}\right)\|C\|. \tag{47}$$

Case 2: When the perturbation simultaneously occurs in both A and F such that

$$(A + \Delta A)(C + \Delta C) = F + \Delta F. \tag{48}$$

Subtracting $AC = F$ from (48) gives

$$A\Delta C + \Delta AC + \Delta A\Delta C = \Delta F.$$

Neglecting the higher order product $\Delta A\Delta C$ and taking the norm on both sides, we have

$$\|\Delta C\| \leq \|A^{-1}\|(\|\Delta F\| + \|\Delta A\|\|C\|). \tag{49}$$

Combining (45) and (49), we get

$$\|\Delta C\| \leq cond(A)\left[\frac{\|\Delta A\|}{\|A\|} + \frac{\|\Delta F\|}{\|F\|}\right]\|C\|.$$

If $cond(A)\left(\frac{\|\Delta A\|}{\|A\|}\right) < 1$ holds, then we have the following sharper bound given as

$$\|\Delta C\| \leq \frac{cond(A)}{\left(1 - cond(A)\left(\frac{\|\Delta A\|}{\|A\|}\right)\right)}\left[\frac{\|\Delta A\|}{\|A\|} + \frac{\|\Delta F\|}{\|F\|}\right]. \tag{50}$$

For numerical computation, we take the ratio

$$p_2 = \frac{\|\Delta C\|\left(1 - cond(A)\left(\frac{\|\Delta A\|}{\|A\|}\right)\right)}{cond(A)\|C\|\left[\frac{\|\Delta A\|}{\|A\|} + \frac{\|\Delta F\|}{\|F\|}\right]}.$$

Value $p_2 \leq 1$ confirms that the theoretical stability bound is satisfied.

Substituting (50) in (42), we get

$$\|u(s,t) - u^P(s,t)\|$$

$$\leq |E(s,t)| + \Phi(s)\Phi(t)\frac{cond(A)}{\left(1 - cond(A)\left(\frac{\|\Delta A\|}{\|A\|}\right)\right)}\left[\frac{\|\Delta A\|}{\|A\|} + \frac{\|\Delta F\|}{\|F\|}\right].$$

□

7.1 Effect of resolution parameters on stability

The stability bounds derived in Theorem (2)show the dependence on the choice of the resolution parameters (M_1, M_2) and index (k_1, k_2). These parameters affect the stability in two distinct ways:

1. **Wavelet basis norm inflation:** Clearly the term $\Phi(s)$ and $\Phi(t)$ are present in both the cases of stability proof. This term depends on M_1, M_2, k_1, and k_2. Consequently, the norms $\Phi(s)$ and $\Phi(t)$ scale monotonically with the increase in the degree of Chelyshkov wavelets. Hence, an increase in resolution parameters increases the value of norms available for error amplification.

2. **Explosion of condition number and the singular barrier:** As the resolution parameters M_1 and M_2 increase the rows of the global matrix A become increasingly linearly dependent. As a result, the condition number grows rapidly, and the large condition number makes the system hyper-sensitive. Also, from the above theorem of stability, the condition for the global matrix A must be $cond(A) < \frac{\|A\|}{\|\Delta A\|}$. Exceeding this limit causes exponential round-off error propagation. Therefore, while higher values of M_1 and M_2 minimize truncation errors, they also increase the system's sensitivity to input data and perturbations in the coefficient matrix. Hence, selecting optimal resolution parameters is necessary to maintain truncation error while ensuring round-off stability.

8 Convergence analysis

Theorem 3. For a positive integers k_1, k_2, the series solution $\mathcal{U}^{\alpha,\beta}_{k_1,k_2,M_1,M_2}$ converges to the exact solution $\mathcal{U}(s,t)$ as $M_1, M_2 \to \infty$.

Proof. For this, we have to prove that $\mathcal{U}^{\alpha,\beta}_{k_1,k_2,M_1,M_2}(s,t)$ is a Cauchy sequence and it converges to $\mathcal{U}(s,t)$. Let $\hat{M}_1 > M_1$, $\hat{M}_2 > M_2$, and $\Lambda = [0,1) \times [0,1)$. We have

$$\mathcal{U}^{\alpha,\beta}_{k_1,k_2,\hat{M}_1,\hat{M}_2}(s,t) - \mathcal{U}^{\alpha,\beta}_{k_1,k_2,M_1,M_2}(s,t)$$

$$= \sum_{n_1=1}^{2^{k_1-1}} \sum_{n_2=1}^{2^{k_2-1}} \sum_{m_1=M_1}^{\hat{M}_1-1} \sum_{m_2=M_2}^{\hat{M}_2-1} r_{n_1,n_2,m_1,m_2} \psi^{\alpha}_{n_1,m_1}(s) \psi^{\beta}_{n_2,m_2}(t),$$

$$\begin{aligned} &\|\mathcal{U}^{\alpha,\beta}_{k_1,k_2,\hat{M}_1,\hat{M}_2}(s,t) - \mathcal{U}^{\alpha,\beta}_{k_1,k_2,M_1,M_2}(s,t)\|_{L^2(\Lambda)} \\ &= \sum_{n_1=1}^{2^{k_1-1}} \sum_{n_2=1}^{2^{k_2-1}} \sum_{m_1=M_1+1}^{\hat{M}_1-1} \sum_{m_2=M_2+1}^{\hat{M}_2-1} \mid r_{n_1,n_2,m_1,m_2} \mid^2, \end{aligned} \tag{51}$$

$$\begin{aligned} &\sum_{n_1=1}^{\infty} \sum_{n_2=1}^{\infty} \sum_{m_1=0}^{\infty} \sum_{m_2=0}^{\infty} \mid r_{n_1,n_2,m_1,m_2} \mid^2 \\ &= \sum_{n_1=1}^{\infty} \sum_{n_2=1}^{\infty} \sum_{m_1=0}^{\infty} \sum_{m_2=0}^{\infty} \mid \left\langle \mathcal{U}(s,t), \psi^{\alpha}_{n_1,m_1}(s) \psi^{\beta}_{n_2,m_2}(t) \right\rangle \mid^2 \\ &\le \|\mathcal{U}\|^2 < \infty. \end{aligned}$$

This implies $\sum_{n_1=1}^{\infty} \sum_{n_2=1}^{\infty} \sum_{m_1=0}^{\infty} \sum_{m_2=0}^{\infty} \mid r_{n_1,n_2,m_1,m_2} \mid^2$ is convergent and hence the term on the left side of (51) tends to 0 as $M_1, M_2 \to \infty$. We have $\left\{\mathcal{U}^{\alpha,\beta}_{k_1,k_2,M_1,M_2}(s,t)\right\}_{M_1,M_2 \in \mathbb{N}}$ is a Cauchy sequence in $L^2(\Lambda)$ and since $L^2(\Lambda)$ is a Hilbert space and hence complete, there exists a function $\mathcal{V}(s,t)$ in $L^2(\Lambda)$ such that

$$\mathcal{U}^{\alpha,\beta}_{k_1,k_2,M_1,M_2}(s,t) \to \mathcal{V}(s,t).$$

Now, we have to show that $\mathcal{U}(s,t) = \mathcal{V}(s,t)$. For this, we have

$$\begin{aligned} &\left\langle \mathcal{V}(s,t) - \mathcal{U}(s,t), \psi^{\alpha}_{n_1,m_1}(s) \psi^{\beta}_{n_2,m_2}(t) \right\rangle \\ &= \left\langle \mathcal{V}(s,t), \psi^{\alpha}_{n_1,m_1}(s) \psi^{\beta}_{n_2,m_2}(t) \right\rangle - \left\langle \mathcal{U}(s,t), \psi^{\alpha}_{n_1,m_1}(s) \psi^{\beta}_{n_2,m_2}(t) \right\rangle \\ &= \lim_{\substack{k_1,k_2 \to \infty \\ M_1,M_2 \to \infty}} \left\langle \mathcal{U}^{\alpha,\beta}_{k_1,k_2,M_1,M_2}(s,t), \psi^{\alpha}_{n_1,m_1}(s) \psi^{\beta}_{n_2,m_2}(t) \right\rangle - r_{n_1,n_2,m_1,m_2} \\ &= r_{n_1,n_2,m_1,m_2} - r_{n_1,n_2,m_1,m_2} \\ &= 0. \end{aligned}$$

Therefore $\mathcal{U}^{\alpha,\beta}_{k_1,k_2,M_1,M_2}$ converges to $\mathcal{U}(s,t)$ as $M_1, M_2 \to \infty$. □

9 Error analysis

Suppose that $\mathcal{U}^{\alpha,\beta}_{k_1,k_2,M_1,M_2}(s,t)$ is the best approximation to $\mathcal{U}(s,t) \in L^2(\Lambda)$ out of the linear space

$$\begin{aligned}&\mathcal{O}^{\alpha,\beta}_{k_1,k_2,M_1,M_2}\\&= span\left(\psi^{\alpha}_{n_1,m_1}(s)\psi^{\beta}_{n_2,m_2}(t) | 1 \le n_j \le 2^{k_j-1}; 0 \le m_j \le M_j - 1, j = 1,2\right),\end{aligned}$$

where $\Lambda = ([0,1) \times [0,1))$ and $\psi^{\alpha}_{n,m}(s)$ denotes the fractional Chelyshkov wavelet.

Lemma 2. Let ${}^C_0D^{i\alpha}_s({}^C_0D^{j\beta}_t\mathcal{U}(s,t)) \in C(\Lambda)$ and $|{}^C_0D^{i\alpha}_s({}^C_0D^{j\beta}_t\mathcal{U}(s,t))| \le \mathcal{R}^{\alpha,\beta}_{M_1,M_2}$ for $i = 0,1,\dots,M_1, j = 0,1,\dots,M_2$. The error bound for

$${}^C_0D^{\gamma}_t\mathcal{U}^{\alpha,\beta}_{k_1,k_2,M_1,M_2}(s,t)$$

by using FCW for $M_2\beta > \gamma$ is given as

$$\begin{aligned}&\left\|{}^C_0D^{\gamma}_t\mathcal{U}(s,t) - {}^C_0D^{\gamma}_t\mathcal{U}^{\alpha,\beta}_{k_1,k_2,M_1,M_2}(s,t)\right\|_{L^2(\Lambda)}\\&\le \frac{\mathcal{R}^{\alpha,\beta}_{M_1,M_2}}{\Gamma(M_1\alpha+1)\Gamma(M_2\beta+1-\gamma)\sqrt{(2M_1\alpha+1)(2M_2\beta+1-2\gamma)}}.\end{aligned}$$

Proof. Proof follows from [22]. □

Lemma 3. According to Lemma 2 for $M_1\alpha > 2$, we have the following result:

$$\begin{aligned}&\left\|{}^C_0D^{1}_s\mathcal{U}(s,t) - {}^C_0D^{1}_s\mathcal{U}^{\alpha,\beta}_{k_1,k_2,M_1,M_2}(s,t)\right\|_{L^2(\Lambda)}\\&\le \frac{\mathcal{R}^{\alpha,\beta}_{M_1,M_2}}{\Gamma(M_2\beta+1)\Gamma(M_1\alpha)\sqrt{(2M_2\beta+1)(2M_1\alpha-1)}}.\end{aligned}$$

$$\begin{aligned}&\left\|{}^C_0D^{2}_s\mathcal{U}(s,t) - {}^C_0D^{2}_s\mathcal{U}^{\alpha,\beta}_{k_1,k_2,M_1,M_2}(s,t)\right\|_{L^2(\Lambda)}\\&\le \frac{\mathcal{R}^{\alpha,\beta}_{M_1,M_2}}{\Gamma(M_2\beta+1)\Gamma(M_1\alpha-1)\sqrt{(2M_2\beta+1)(2M_1\alpha-3)}}.\end{aligned}$$

Theorem 4. The error bound $(\mathcal{E}^{m_2,M_2}_{m_1,M_1})$ is given as

$$||\mathcal{E}^{m_2,M_2}_{m_1,M_1}||_{L^2(\Lambda)}$$

$$
\begin{aligned}
&\le \mathcal{R}^{\alpha,\beta}_{M_1,M_2}\Bigg(\frac{1}{\Gamma(M_1\alpha+1)\Gamma(M_2\beta+1-\gamma)\sqrt{(2M_1\alpha+1)(2M_2\beta+1-2\gamma)}}\\
&\quad+\frac{\mathcal{M}_1}{\Gamma(M_2\beta+1)\Gamma(M_1\alpha)\sqrt{(2M_2\beta+1)(2M_1\alpha-1)}}\\
&\quad+\frac{\mathcal{M}_2}{\Gamma(M_2\beta+1)\Gamma(M_1\alpha-1)\sqrt{(2M_2\beta+1)(2M_1\alpha-3)}}\Bigg),
\end{aligned}
$$

where $\|a(s)\| \le \mathcal{M}_1$ and $\|b(s)\| \le \mathcal{M}_2$.

Proof. We have

$$
\begin{aligned}
\|\mathcal{E}^{m_2,M_2}_{m_1,M_1}\|_{L^2(\Lambda)} =&\|{}^C_0D^\gamma_t\mathcal{U}^{\alpha,\beta}_{k_1,k_2,M_1,M_2}(s,t)+a(s){}^C_0D^1_s\mathcal{U}^{\alpha,\beta}_{k_1,k_2,M_1,M_2}(s,t)\\
&+b(s){}^C_0D^2_s\mathcal{U}^{\alpha,\beta}_{k_1,k_2,M_1,M_2}(s,t)-f(s,t)\|
\end{aligned}
$$

Using (22), we get

$$
\begin{aligned}
\|\mathcal{E}^{m_2,M_2}_{m_1,M_1}\|_{L^2(\Lambda)} =&\|{}^C_0D^\gamma_t\mathcal{U}^{\alpha,\beta}_{k_1,k_2,M_1,M_2}(s,t)+a(s){}^C_0D^1_s\mathcal{U}^{\alpha,\beta}_{k_1,k_2,M_1,M_2}(s,t)\\
&+b(s){}^C_0D^2_s\mathcal{U}^{\alpha,\beta}_{k_1,k_2,M_1,M_2}(s,t)\\
&-{}^C_0D^\gamma_t\mathcal{U}(s,t)-a(s){}^C_0D^1_s\mathcal{U}(s,t)-b(s){}^C_0D^2_s\mathcal{U}(s,t)\|\\
\le&\|{}^C_0D^\gamma_t\mathcal{U}^{\alpha,\beta}_{k_1,k_2,M_1,M_2}(s,t)-{}^C_0D^\gamma_t\mathcal{U}(s,t)\|\\
&+\|a(s)\|\|{}^C_0D^1_s\mathcal{U}^{\alpha,\beta}_{k_1,k_2,M_1,M_2}(s,t)-{}^C_0D^1_s\mathcal{U}(s,t)\|\\
&+\|b(s)\|\|{}^C_0D^2_s\mathcal{U}^{\alpha,\beta}_{k_1,k_2,M_1,M_2}(s,t)-{}^C_0D^2_s\mathcal{U}(s,t)\|.
\end{aligned}
$$

Using Lemmas 2 and 3, we have

$$
\begin{aligned}
\|\mathcal{E}^{m_2,M_2}_{m_1,M_1}\|_{L^2(\Lambda)} \le&\frac{\mathcal{R}^{\alpha,\beta}_{M_1,M_2}}{\Gamma(M_1\alpha+1)\Gamma(M_2\beta+1-\gamma)\sqrt{(2M_1\alpha+1)(2M_2\beta+1-2\gamma)}}\\
&+\mathcal{M}_1\frac{\mathcal{R}^{\alpha,\beta}_{M_1,M_2}}{\Gamma(M_2\beta+1)\Gamma(M_1\alpha)\sqrt{(2M_2\beta+1)(2M_1\alpha-1)}}\\
&+\mathcal{M}_2\frac{\mathcal{R}^{\alpha,\beta}_{M_1,M_2}}{\Gamma(M_2\beta+1)\Gamma(M_1\alpha-1)\sqrt{(2M_2\beta+1)(2M_1\alpha-3)}}.
\end{aligned}
$$

From above, it follows that

$$
\begin{aligned}
&\|\mathcal{E}^{m_2,M_2}_{m_1,M_1}\|_{L^2(\Lambda)}\\
&\le \mathcal{R}^{\alpha,\beta}_{M_1,M_2}\Bigg(\frac{1}{\Gamma(M_1\alpha+1)\Gamma(M_2\beta+1-\gamma)\sqrt{(2M_1\alpha+1)(2M_2\beta+1-2\gamma)}}
\end{aligned}
$$

$$+\frac{\mathcal{M}_1}{\Gamma(M_2\beta+1)\Gamma(M_1\alpha)\sqrt{(2M_2\beta+1)(2M_1\alpha-1)}}$$
$$+\frac{\mathcal{M}_2}{\Gamma(M_2\beta+1)\Gamma(M_1\alpha-1)\sqrt{(2M_2\beta+1)(2M_1\alpha-3)}}\Bigg).$$

Therefore as $M_1, M_2 \to \infty$

$$\|\mathcal{E}_{m_1,M_1}^{m_2,M_2}\|_{L^2(\Lambda)} \to 0.$$

Also, if k_1, $k_2 \to \infty$, then

$$\left|\left(\frac{n_1}{2^{k_1-1}}\right)^{\frac{1}{\alpha}} - \left(\frac{n_1-1}{2^{k_1-1}}\right)^{\frac{1}{\alpha}}\right| \to 0, \left|\left(\frac{n_2}{2^{k_2-1}}\right)^{\frac{1}{\beta}} - \left(\frac{n_2-1}{2^{k_2-1}}\right)^{\frac{1}{\beta}}\right| \to 0.$$

This implies

$$\|\mathcal{E}_{m_1,M_1}^{m_2,M_2}\|_{L^2(\Lambda)} \to 0.$$

□

10 Numerical examples

In this section, we investigate the accuracy of the proposed method using six numerical examples. All computations are performed using Wolfram Mathematica 12.0. The resulting linear algebraic systems obtained after applying the proposed method are solved using the LinearSolve command in Mathematica. The computations are handled by Mathematica's default machine-precision arithmetic. In one numerical example, errors as low as 10^{-19} are interpreted as agreement at the level of machine precision. The condition number in that case is 1381.17. A condition number of this magnitude indicates that the system is well-conditioned and that round-off errors are negligibly amplified. We have taken $k_1 = k_2 = k$ and $M_1 = M_2 = M$, and $n = 2^{k-1}M$ denotes the number of basis functions. The formula for absolute error is

$$\mathcal{E}(s,t) = \mid u(s,t) - \mathcal{U}(s,t) \mid, \tag{52}$$

where $\mathcal{U}(s,t)$, $u(s,t)$ denote the exact and approximate solutions, respectively.

Example 1. Consider the following TFCDE:

$$\frac{\partial^\gamma \mathcal{U}(s,t)}{\partial t^\gamma} - \frac{\partial^2 \mathcal{U}(s,t)}{\partial s^2} = 2\left(\frac{1}{\Gamma(3-\gamma)} t^{2-\gamma} - 1\right), \tag{53}$$

with I.C and B.Cs

$$\mathcal{U}(s,0) = s^2, \quad s \in (0,1), \qquad \mathcal{U}(0,t) = t^2, \quad \mathcal{U}(1,t) = 1 + t^2, \quad t \in (0,1].$$

The exact solution is given as

$$\mathcal{U}(s,t) = s^2 + t^2. \tag{54}$$

Table 1 compares the absolute error of the proposed method with BFM [7] and FWM [38] at $\alpha = \beta = 1$, $\gamma = 0.5$, and $t = 0.25$. In Table 2, we present the absolute error of the proposed method for different values of γ and compare it with FWM [38]. These tables show that the proposed method gives better results with a small number of basis functions. To evaluate the computational efficiency of the proposed method, Table 3 presents the maximum absolute error, CPU time, and memory usage for different values of the resolution parameters. Clearly, CPU time and memory usage increase with higher resolution parameters. To confirm the numerical stability of the proposed method, Table 4 presents the logarithmic condition number and stability measures (p_1, p_2) for different values of n. The condition number increases with an increase in n, indicating greater sensitivity of the numerical system to perturbations. The stability parameters $p_1 \leq 1$ and $p_2 \leq 1$ are satisfied for different n, confirming the stability of the proposed method. Figure 1 shows the plot of exact, approximate, and absolute error with $\alpha = \beta = 0.1$ and $\gamma = 0.8$.

Table 1: Comparison of $\mathcal{E}(s,t)$ of Example 1 at $\alpha = \beta = 1$, $\gamma = 0.5$, and $t = 0.25$.

s	BFM [7]			FWM [38]		Proposed method
	$j = 1, m = 2$	$j = 1, m = 3$	$j = 2, m = 2$	$k = 2, M = 3$	$k = 3, M = 4$	$k = 2,\ M = 3$
0.2	3.3e-02	4.4e-03	8.8e-02	2.0561e-04	6.3909e-05	1.10834e-08
0.4	1.9e-04	5.1e-02	9.8e-02	5.2032e-04	8.6140e-05	4.62512e-08
0.6	1.6e-02	7.1e-02	3.4e-01	9.9285e-05	2.541e-04	1.07939e-07
0.8	1.2e-01	2.8e-02	4.3e-01	9.9285e-05	5.6495e-07	2.05404e-07

Example 2. Consider the following TFCDE:

$$\frac{\partial^\gamma \mathcal{U}(s,t)}{\partial t^\gamma} + s\frac{\partial \mathcal{U}(s,t)}{\partial s} + \frac{\partial^2 \mathcal{U}(s,t)}{\partial s^2} = 2t^\gamma + 2s^2 + 2, \tag{55}$$

with I.C and B.Cs

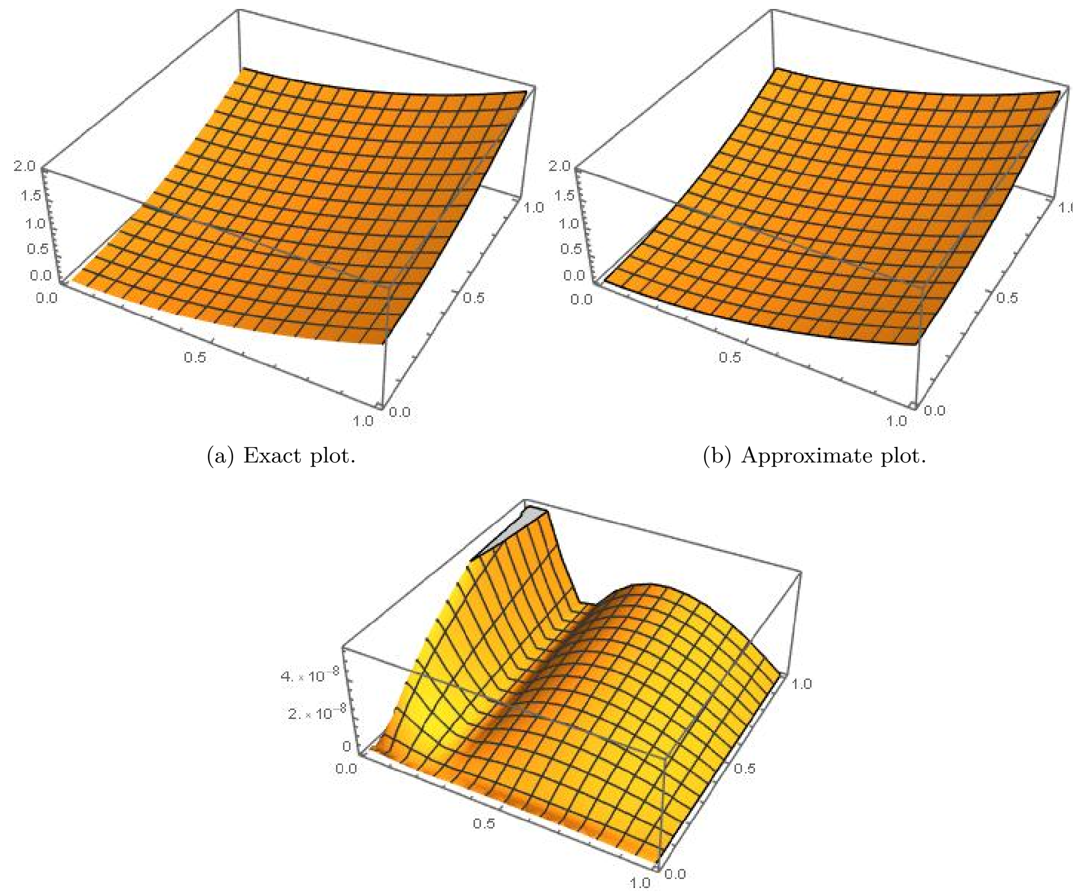

(a) Exact plot.

(b) Approximate plot.

(c) Absolute error plot.

Figure 1: Plot of exact, approximate, and absolute error of Example 1 with $\alpha = \beta = 0.1$, $\gamma = 0.8$.

$$\mathcal{U}(s,0) = s^2, \quad s \in (0,1),$$

$$\mathcal{U}(0,t) = \frac{2\Gamma(\gamma+1)}{\Gamma(2\gamma+1)} t^{2\gamma}, \qquad \mathcal{U}(1,t) = 1 + \frac{2\Gamma(\gamma+1)}{\Gamma(2\gamma+1)} t^{2\gamma}, \quad t \in (0,1].$$

The exact solution is given as

$$\mathcal{U}(s,t) = s^2 + \frac{2\Gamma(\gamma+1)}{\Gamma(2\gamma+1)} t^{2\gamma}. \tag{56}$$

Table 5 shows a comparison of the absolute error of the proposed method with the methods in [24], [2], [26], and [38]. This table confirms that the proposed method performs better than the other methods, and the fractional power in the Chelyshkov wavelet makes it more accurate. Table 6 shows the maximum absolute error, CPU time, and memory used for different values

Table 2: Comparison of $\mathcal{E}(s,t)$ of Example 1 for different values of γ.

(s,t)	FWM [38] $(k=3, M=4)$ $\gamma=0.8$	$\gamma=0.9$	Proposed method $(k=2, M=3)$ $\alpha=\beta=0.1$, $\gamma=0.8$	$\alpha=\beta=0.1$, γ=0.9
(0.1,0.1)	4.1858e-08	7.4698e-07	7.14461e-09	5.01525e-09
(0.2,0.2)	6.6925e-07	2.8060e-07	3.66583e-09	2.79564e-09
(0.3,0.3)	7.5506e-08	1.2633e-08	4.97482e-09	3.99839e-09
(0.4,0.4)	8.8604e-07	8.1873e-08	1.33681e-08	1.07923e-08
(0.5,0.5)	4.1223e-08	2.4966e-06	1.95202e-08	1.58519e-08
(0.6,0.6)	4.2531e-06	1.3715e-08	2.26026e-08	1.243881e-08
(0.7,0.7)	9.9860e-08	1.4136e-08	2.22673e-08	1.32283e-08
(0.8,0.8)	1.3350e-08	2.1795e-08	1.33388e-08	1.5095e-08
(0.9,0.9)	4.0122e-07	9.3121e-09	1.09523e-08	9.01145e-09

Table 3: Maximum absolute error, CPU time, and memory used for different values of k and M with $\alpha=\beta=0.1$ and $\gamma=0.8$.

	Maximum Absolute Error	CPU Time (seconds)	Memory used (MB)
$k=2, M=3$	4.34443e-07	6.641	2.82407
$k=2, M=4$	1.80993e-07	14.203	9.40698
$k=2, M=5$	1.30899e-07	15.213	21.6597
$k=3, M=4$	1.02445e-08	19.313	50.2342

of k and M with $\alpha=\beta=1, \gamma=0.5$. Table 7 presents the logarithmic condition number and numerical stability parameters for $\alpha=\beta=0.1$ and $\gamma=0.5$, which confirm the numerical stability of the proposed method. Figure 2 shows the plot of exact, approximate, and absolute error for $\alpha=\beta=0.1$, $\gamma=0.5$, $k=2$, and $M=3$.

Example 3. Consider the following TFCDE:

$$\frac{\partial^\gamma \mathcal{U}(s,t)}{\partial t^\gamma}+\frac{\partial \mathcal{U}(s,t)}{\partial s}-s\frac{\partial^2 \mathcal{U}(s,t)}{\partial s^2}=f(s,t), \tag{57}$$

with I.C and B.Cs

$$\mathcal{U}(s,0)=e^s, \quad s\in(0,1),$$

$$\mathcal{U}(0,t)=(t^2+1)(1-t), \qquad \mathcal{U}(1,t)=(t^2+1)(e-t), \quad t\in(0,1],$$

Table 4: The value of logarithmic condition number and numerical stability parameters with $\alpha = \beta = 0.1$, $\gamma = 0.8$ using relative perturbations $\frac{\|\Delta A\|}{\|A\|} = 10^{-10}$ and $\frac{\|\Delta F\|}{\|F\|} = 10^{-04}$.

n	$\log_{10}(cond(A))$	p_1	p_2
4	5.7190	3.77442×10^{-02}	3.77422×10^{-02}
6	6.9592	2.18827×10^{-03}	2.18627×10^{-03}
8	9.3294	7.40171×10^{-06}	5.81816×10^{-06}
10	9.4165	5.35671×10^{-06}	5.25612×10^{-06}

Table 5: Comparison of $\mathcal{E}(s,t)$ of Example 2 at $\gamma = 0.5$, $t = 0.5$.

(s,t)	Sinc-Legendre [24]		B-spline Sinc [2]		Chebyshev [26]	FWM [38]	Proposed method	
	$n = 15$	$n = 25$	$n = 5$	$n = 20$	$n = 5$	$n = 16$	$n = 6$, $\alpha = \beta = 1$	$n = 6$, $\alpha = \beta = 0.1$
0.1	6.994e-05	6.462e-06	6.481e-04	1.369e-09	7.964e-06	3.6637e-15	6.1886e-19	3.71677e-19
0.2	1.721e-04	1.578e-05	4.109e-04	7.591e-10	3.912e-06	1.1102e-14	9.07256e-19	1.83842e-19
0.3	2.472e-04	2.272e-05	5.493e-04	1.184e-09	6.162e-06	8.8818e-16	1.39548e-18	4.91185e-19
0.4	2.912e-04	2.674e-05	5.198e-04	1.068e-09	5.953e-06	5.1071e-15	2.08354e-18	6.42139e-19
0.5	3.004e-04	2.759e-05	4.912e-04	9.819e-10	2.103e-06	4.4409e-16	3.56819e-18	6.85571e-19
0.6	2.760e-04	2.534e-05	5.063e-04	1.039e-09	7.639e-06	2.2204e-16	3.35632e-18	6.49804e-19
0.7	2.213e-04	2.035e-05	5.045e-04	1.031e-09	1.967e-06	0	0	0
0.8	1.440e-04	1.320e-05	5.040e-04	1.030e-09	8.103e-06	0	0	0
0.9	5.026e-05	4.653e-06	5.037e-04	1.031e-09	6.019e-06	0	0	0

and $f(s,t) = \frac{2t^{2-\gamma}}{\Gamma(3-\gamma)}e^s - \frac{t^{1-\gamma}}{\Gamma(2-\gamma)} - \frac{6t^{3-\gamma}}{4-\gamma} + (t^2+1)(1-s)e^s$.

The exact solution is given as

$$\mathcal{U}(s,t) = (t^2+1)(e^s - t). \tag{58}$$

We have used the proposed method to solve the above problem for $k = 2$ and $M = 3$. The comparison of the absolute error with the method in [41] for various values of γ is reported in Table 8. Table 9 shows the maximum absolute error, CPU time, and memory used for different values of k and M with $\alpha = \beta = \gamma = 0.3$. Table 10 confirms the numerical stability of the proposed method. Figure 3 shows the plot of exact and approximate solutions for $\alpha = \beta = 1, \gamma = 0.9$, $k = 2$, and $M = 3$.

Example 4. Consider the following TFCDE:

$$\frac{\partial^\gamma \mathcal{U}(s,t)}{\partial t^\gamma} + t^2 e^s \frac{\partial \mathcal{U}(s,t)}{\partial s} - (s^2+t+1)\frac{\partial^2 \mathcal{U}(s,t)}{\partial s^2} = f(s,t), \tag{59}$$

with I.C and B.Cs

Table 6: Maximum absolute error, CPU time, and memory used for different values of k and M with $\alpha = \beta = 1, \gamma = 0.5$.

	Maximum Absolute Error	CPU Time (seconds)	Memory used (MB)
$k = 2, M = 3$	3.76595e-18	8.767	1.34804
$k = 2, M = 4$	1.19022e-19	16.531	3.46304
$k = 2, M = 5$	1.03654e-19	35.121	7.53673
$k = 3, M = 3$	1.00454e-19	47.528	8.23176

Table 7: The value of logarithmic condition number and numerical stability parameters with $\alpha = \beta = 0.1$, $\gamma = 0.5$ using relative perturbations $\frac{\|\Delta A\|}{\|A\|} = 10^{-10}$ and $\frac{\|\Delta F\|}{\|F\|} = 10^{-04}$.

n	$\log_{10}(cond(A))$	p_1	p_2
4	4.1318	1.3326×10^{-02}	1.21996×10^{-02}
6	5.9837	2.0292×10^{-02}	2.0292×10^{-02}
8	8.2712	1.07868×10^{-04}	1.05834×10^{-04}
10	8.6376	1.61878×10^{-06}	1.53048×10^{-05}

Table 8: Comparison of absolute errors for Example 3 with $\alpha = \beta = \gamma$.

(s,t)	Method in [41] ($k = 2, M = 6$)			Proposed method ($k = 2, M = 3$)		
	$\gamma = 0.3$	$\gamma = 0.5$	$\gamma = 0.9$	$\gamma = 0.3$	γ=0.5	$\gamma = 0.9$
(0.1,0.1)	7.75e-06	1.20e-05	2.55e-05	2.71477e-06	2.42987e-06	4.63002e-06
(0.2,0.2)	1.70e-05	2.33e-05	3.50e-05	3.80907e-06	1.13041e-05	1.02384e-05
(0.3,0.3)	2.44e-05	3.02e-05	2.55e-05	5.05275e-06	2.67296e-05	1.51364e-05
(0.4,0.4)	2.87e-05	3.37e-05	2.71e-05	5.19807e-06	3.0366e-05	1.70165e-06
(0.5,0.5)	3.03e-05	3.31e-05	2.07e-05	4.7934e-06	8.16393e-06	1.94832e-06
(0.6,0.6)	2.88e-05	3.00e-05	1.51e-05	4.07959e-06	9.31634e-06	1.48382e-06
(0.7,0.7)	2.45e-05	2.45e-05	1.03e-05	3.18235e-06	6.03367e-06	1.33323e-06
(0.8,0.8)	1.79e-05	1.73e-05	6.27e-06	2.175e-06	3.51789e-06	1.22325e-06
(0.9,0.9)	9.58e-06	8.97e-06	2.91e-06	1.10383e-06	1.32524e-06	8.7549e-07

$$\mathcal{U}(s,0) = s^2, \quad s \in (0,1), \qquad \mathcal{U}(0,t) = t^2, \qquad \mathcal{U}(1,t) = 1 + t^2, \quad t \in (0,1],$$

and $f(s,t) = \frac{2t^{2-\gamma}}{\Gamma(3-\gamma)} - 2(s^2 + t + 1) + 2t^2 s e^s$.

The exact solution is given as

$$\mathcal{U}(s,t) = s^2 + t^2. \tag{60}$$

Table 11 shows the absolute error for different values of α, β, γ, indicating that the fractional power of the Chelyshkov wavelet yields a more accurate result. Table 12 shows the maximum absolute error, CPU time, and memory used for different values of k and M with $\alpha = \beta = \gamma = 0.1$.

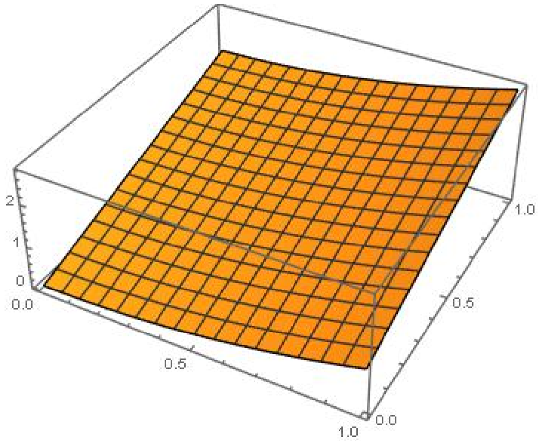

(a) Exact plot.

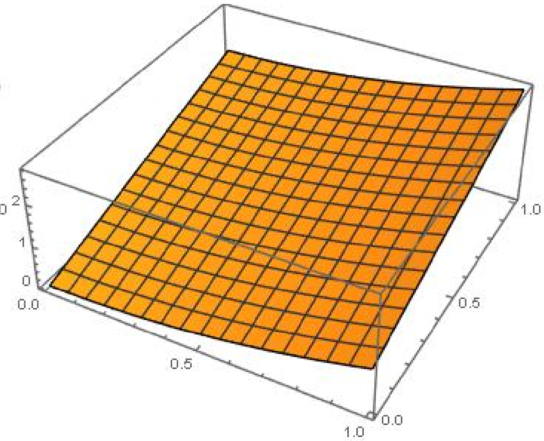

(b) Approximate plot.

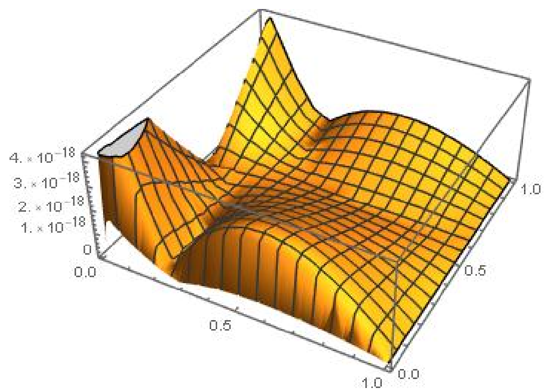

(c) Absolute error plot.

Figure 2: Plot of the exact, approximate, and absolute error of Example 2.

Table 13 confirms the numerical stability of the proposed method. Figure 4 shows the graph of exact, approximate, and absolute error for $\alpha = \beta = \gamma = 0.1$, $k = 2$, and $M = 3$; it is clear that by employing a few terms of fractional-order Chelyshkov wavelets, we can obtain a good approximation of the exact solution.

Example 5. Consider the following TFCDE:

$$\frac{\partial^\gamma \mathcal{U}(s,t)}{\partial t^\gamma} + (1+0.5s)\frac{\partial \mathcal{U}(s,t)}{\partial s} - 0.2(1+s^2)\frac{\partial^2 \mathcal{U}(s,t)}{\partial s^2} = 0, \tag{61}$$

with I.C and B.Cs

Table 9: Maximum absolute error, CPU time, and memory used for different values of k and M with $\alpha = \beta = \gamma = 0.3$.

	Maximum Absolute Error	CPU Time (seconds)	Memory used (MB)
$k = 2, M = 3$	5.28105e-06	8.126	4.47313
$k = 2, M = 4$	2.3214e-06	9.283	34.618
$k = 2, M = 5$	1.73625e-06	19.818	50.9134
$k = 3, M = 3$	3.26535e-07	39.238	61.2142

Table 10: The value of logarithmic condition number and numerical stability parameters with $\alpha = \beta = \gamma = 0.3$ using relative perturbations $\frac{\|\Delta A\|}{\|A\|} = 10^{-10}$ and $\frac{\|\Delta F\|}{\|F\|} = 10^{-04}$.

n	$\log_{10}(cond(A))$	p_1	p_2
4	3.8886	1.47854×10^{-01}	1.35767×10^{-01}
6	5.5562	5.55557×10^{-02}	5.55558×10^{-02}
8	7.6073	3.9012×10^{-04}	3.88542×10^{-04}
10	7.8183	5.2348×10^{-06}	5.1574×10^{-06}

Table 11: The absolute error of Example 4 with $k = 2, M = 3$, and $t = 0.1$.

	$\alpha = \beta = 1$		$\alpha = \beta = \gamma$	
s	$\gamma = 0.1$	$\gamma = 0.3$	$\gamma = 0.1$	$\gamma = 0.3$
0.1	2.83606e-04	3.02301e-04	4.92041e-05	3.63389e-05
0.2	5.51765e-04	5.86786e-04	2.31822e-05	5.27762e-05
0.3	7.88299e-04	8.35926e-04	6.04444e-05	8.46832e-05
0.4	9.93208e-04	1.04971e-03	4.63942e-05	9.33962e-04
0.5	8.80454e-04	9.11348e-04	1.06622e-04	8.98575e-04
0.6	1.22125e-03	1.27917e-03	1.31595e-05	7.889486e-04
0.7	1.16542e-03	1.21533e-03	1.2884e-05	6.3249e-04
0.8	9.43269e-04	9.80856e-04	1.03605e-05	4.442731e-05
0.9	5.54796e-04	5.75745e-04	5.97019e-05	2.29777e-05

$$\mathcal{U}(s,0) = e^{-10s}, \quad s \in (0,1), \qquad \mathcal{U}(0,t) = 1, \qquad \mathcal{U}(1,t) = e^{-10}, \quad t \in (0,1].$$

Here $\mathcal{U}(s,t)$ denotes the pollutant concentration, $1 + 0.5s$ denotes spatially varying groundwater velocity, and $0.2(1 + s^2)$ is a spatially varying diffusion coefficient. The initial condition shows that the pollutant concentration is highest near the inlet ($s = 0$) and decays exponentially along the flow direction. The boundary condition indicates that a constant pollutant source of concentration 1 is maintained at the inlet, and the outlet concentration is fixed at e^{-10}. The fractional order $0 < \gamma < 1$ denotes anomalous transport with a memory effect due to trapping and heterogeneous pore structures, and $\gamma = 1$ shows the classical transport. The exact solution

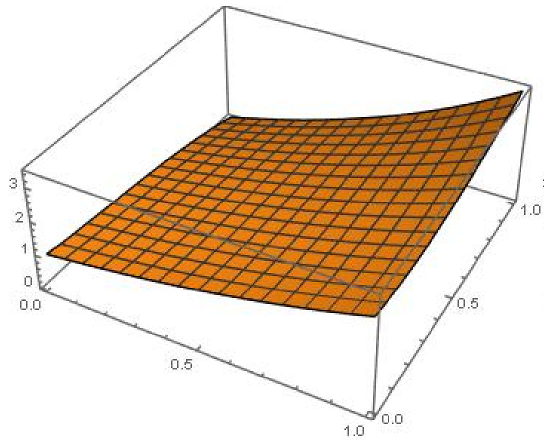

(a) Exact plot.

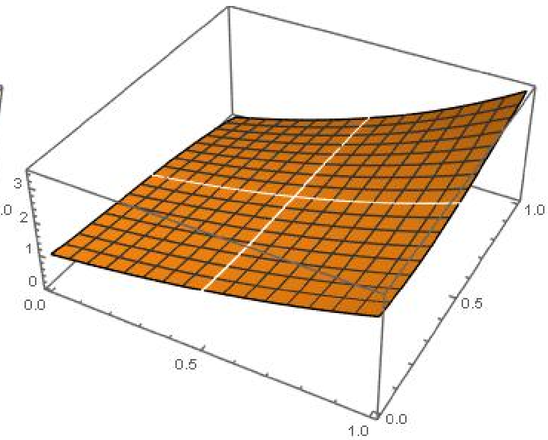

(b) Approximate plot.

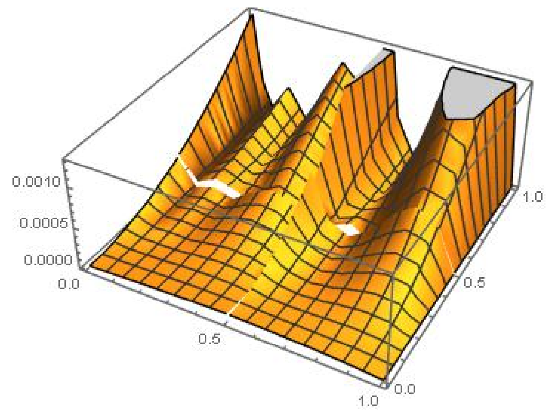

(c) Absolute error plot.

Figure 3: Plot of exact, approximate, and absolute error of Example 3.

of the governing equation is not known. Therefore, the proposed wavelet method is employed to obtain an approximate solution. The accuracy of the numerical scheme is assessed by comparing successive approximations obtained with different wavelet resolutions. Table 14 presents the error values obtained by subtracting the numerical solutions corresponding to $k = 1, M = 7$ and $k = 1, M = 8$ at selected spatial and temporal points with $\alpha = \beta = 1$ and $\gamma = 0.8$. Table 15 shows the maximum absolute error, CPU time, and memory used for different values of k and M. The value of logarithmic condition number and numerical stability parameters in Table 16 with $\alpha = \beta = 1, \gamma = 0.8$ using relative perturbations $\frac{\|\Delta A\|}{\|A\|} = 10^{-10}$ and $\frac{\|\Delta F\|}{\|F\|} = 10^{-04}$ confirms the stability of the proposed method. Figure 5 shows the plot of the approximate solution for different values of M with $\alpha = \beta = 1$, and $\gamma = 0.8$.

Table 12: Maximum absolute error, CPU time, and memory used for different values of k and M with $\alpha = \beta = \gamma = 0.1$.

	Maximum Absolute Error	CPU Time (seconds)	Memory used (MB)
$k = 2, M = 3$	4.99892e-04	7.999	1.60871
$k = 2, M = 4$	5.32841e-05	8.016	3.3327
$k = 2, M = 5$	3.79412e-06	8.234	7.2016
$k = 3, M = 3$	1.21131e-07	10.412	8.04546

Table 13: The value of logarithmic condition number and numerical stability parameters with $\alpha = \beta = \gamma = 0.1$ using relative perturbations $\frac{\|\Delta A\|}{\|A\|} = 10^{-10}$ and $\frac{\|\Delta F\|}{\|F\|} = 10^{-04}$.

n	$\log_{10}(cond(A))$	p_1	p_2
4	3.4931	1.67239×10^{-01}	1.67219×10^{-01}
6	4.9017	2.87983×10^{-01}	2.8798×10^{-01}
8	6.1741	2.87199×10^{-02}	2.87156×10^{-02}
10	6.9410	2.18385×10^{-03}	2.18194×10^{-03}

Table 14: The value of error at different spatial and temporal points with $\alpha = \beta = 1$ and $\gamma = 0.8$.

s	$t = 0.25$	$t = 0.50$	$t = 0.75$	$t = 1.00$
0.1	3.52011e-03	3.35035e-03	9.91772e-03	4.82175e-02
0.2	1.380097e-02	1.1367e-04	1.0585599e-02	8.173366e-02
0.3	1.443829e-02	4.84574e-03	1.684423e-02	9.650087e-02
0.4	1.373029e-02	9.63895e-03	2.093999e-02	9.766614e-02
0.5	1.670874e-02	9.20784e-03	1.893917e-02	8.86383e-02
0.6	1.920814e-02	7.58296e-03	1.574153e-02	2.154644e-02
0.7	1.637163e-02	9.18778e-03	1.608100e-02	7.313191e-02
0.8	1.171127e-02	9.72846e-03	1.535096e-02	6.388752e-02
0.9	1,284100e-02	5.0756e-04	4.09452e-03	3.586075e-02

Example 6. To show the practical applicability of the proposed method, we consider the dispersion of sulfur dioxide (SO_2) in the atmosphere. The transport process is governed by the time-fractional convection-diffusion equation given as

$$\frac{\partial^\gamma \mathcal{U}(s,t)}{\partial t^\gamma} + v\frac{\partial \mathcal{U}(s,t)}{\partial s} - D\frac{\partial^2 \mathcal{U}(s,t)}{\partial s^2} = 0, \tag{62}$$

with I.C and B.Cs

$$\mathcal{U}(s,0) = \sin(\pi s), \quad s \in (0,1), \qquad \mathcal{U}(0,t) = 0, \qquad \mathcal{U}(1,t) = 0, \quad t \in (0,1],$$

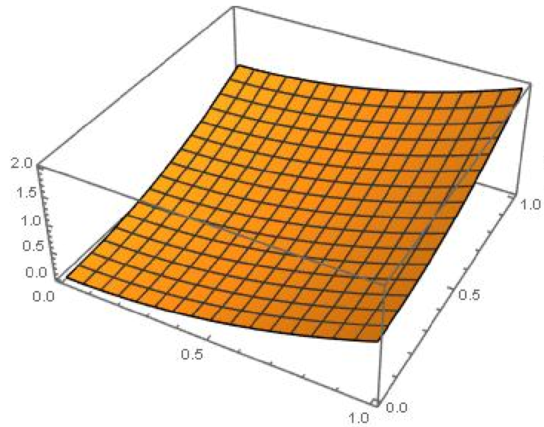

(a) Exact plot.

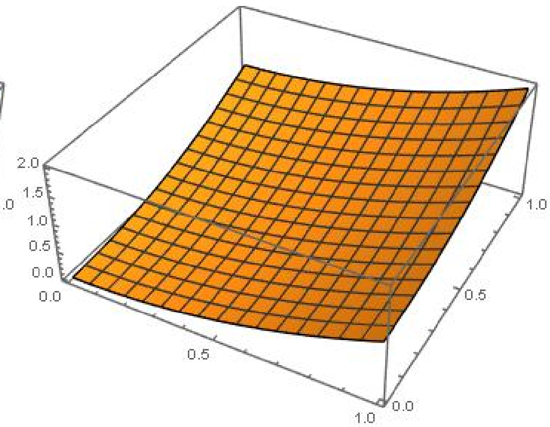

(b) Approximate plot.

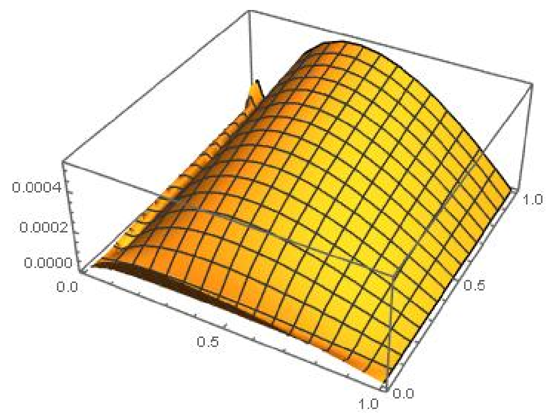

(c) Absolute error plot.

Figure 4: Plot of exact, approximate, and absolute error of Example 4.

where $\mathcal{U}(s,t)$ denotes the pollutant concentration, D is the diffusion coefficient, and v represents the transport velocity. We take $D = 3.6 \times 10^{-4} cm^2/s$ and $v = 3.6 \times 10^{-3} cm/s$ from a recent atmospheric pollution study involving (SO_2) dispersion.

The exact solution of this problem is given as $\mathcal{U}(s,t) = \sin(\pi s)\mathrm{ML}_\gamma\left(-D\pi^2 t^\gamma\right)$, where ML_γ denotes the Mittag-Leffler function. The memory effects in transport processes are captured by the fractional order γ. When $0 < \gamma < 1$, the equation exhibits subdiffusive behavior. In this situation, the pollutants remain trapped for longer periods due to weak atmospheric mixing and stable meteorological conditions. This type of behavior is observed during winter inversions, when pollutants accumulate, leading to poor air quality. When $\gamma = 1$, the transport process is classical diffusion. We have employed FCW to compute the concentration profiles at different times. The

Table 15: Maximum absolute error, CPU time, and memory used for different values of k and M with $\alpha = \beta = 1, \gamma = 0.8$.

	Maximum Absolute Error	CPU Time (seconds)	Memory used (MB)
$k = 1, M = 5$	3.77118e-01	8.468	1.76382
$k = 1, M = 6$	1.02784e-01	8.521	1.99509
$k = 1, M = 7$	9.76661e-02	19.751	2.8343
$k = 2, M = 4$	2.63402e-03	37.469	4.89185
$k = 2, M = 5$	1.09729e-03	38.265	10.5364

Table 16: The value of logarithmic condition number and numerical stability parameters with $\alpha = \beta = 1, \gamma = 0.8$ using relative perturbations $\frac{\|\Delta A\|}{\|A\|} = 10^{-10}$ and $\frac{\|\Delta F\|}{\|F\|} = 10^{-04}$.

n	$\log_{10}(cond(A))$	p_1	p_2
5	2.8305	2.95454×10^{-01}	2.95454×10^{-01}
6	3.4326	1.85343×10^{-01}	1.85343×10^{-01}
7	4.0267	2.34766×10^{-02}	2.34766×10^{-02}
8	4.0326	1.02877×10^{-02}	1.02875×10^{-02}
10	5.2664	5.01782×10^{-03}	5.01782×10^{-03}

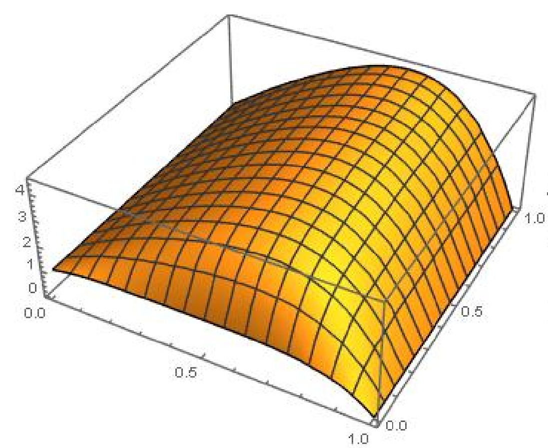

(a) $k = 1, M = 7$.

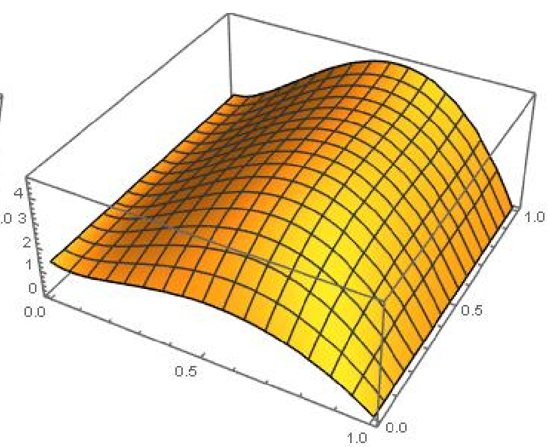

(b) $k = 1, M = 8$.

Figure 5: Plot of approximate solution for different values of M with $\alpha = \beta = 1$ and $\gamma = 0.8$.

numerical results shown in Table 17 indicate that the pollutant concentration decreases over time as convection and diffusion transport it throughout the domain. In Table 18, we have compared the proposed method with the method in [19]. This table shows that the error increases over time and decreases as the γ increases. However, the errors reported in the table are consistently lower than those reported in [19], demonstrating the proposed method's higher accuracy. As shown in

Table 19 the maximum absolute error decreases with an increase in resolution parameters. Table 20 confirms the stability of the proposed method. Figure 6 shows the plot of exact, approximate, and absolute error with $\alpha = \beta = 1, \gamma = 0.8$, $k = 2$, and $M = 3$.

Table 17: The approximate value of concentration $\mathcal{U}(s,t)$ at different points with $\alpha = \beta = 1, \gamma = 0.8$, $k = 2$, and $M = 3$.

s	Concentration $\mathcal{U}(s,t)$					
	$t = 0.0$	$t = 0.2$	$t = 0.4$	$t = 0.6$	$t = 0.8$	$t = 1.0$
0.0	0	0	0	0	0	0
0.2	0.587736	0.587171	0.586709	0.586298	0.585919	0.585562
0.4	0.950978	0.950072	0.949331	0.948668	0.948056	0.947477
0.6	0.950978	0.950069	0.949326	0.949324	0.948656	0.948038
0.8	0.587736	0.587166	0.586698	0.586276	0.585886	0.585515
1.0	0	0	0	0	0	0

Table 18: Comparison of absolute errors for Example 6 with $\alpha = \beta = 1$, and $s = 0.5$.

t	Method in [19]			Proposed method $(k = 2, M = 3)$		
	$\gamma = 0.4$	$\gamma = 0.7$	$\gamma = 1.0$	$\gamma = 0.4$	γ=0.7	$\gamma = 1.0$
0.2	3.972e-03	2.419e-03	1.421e-03	3.02648e-04	2.73726e-05	1.01261e-05
0.4	5.231e-03	3.931e-03	2.842e-03	3.94373e-04	5.18062e-05	5.80978e-06
0.8	6.918e-03	6.378e-03	5.684e-03	4.97679e-04	1.59196e-04	4.68719e-05
1.0	7.564e-03	7.467e-03	7.564e-03	3.991e-03	3.90017e-03	3.54675e-03

Table 19: Maximum absolute error, CPU time, and memory used for different values of k and M with $\alpha = \beta = 1, \gamma = 0.8$.

	Maximum Absolute Error	CPU Time (seconds)	Memory used (MB)
$k = 2, M = 3$	2.08857e-03	6.016	3.74405
$k = 2, M = 4$	2.07524e-03	16.031	4.19507
$k = 2, M = 5$	2.04201e-03	36.844	7.62554
$k = 3, M = 3$	1.51867e-04	40.365	8.70413

11 Conclusion

In this work, a numerical method based on the fractional Chelyshkov wavelet was introduced for solving the time fractional convection-diffusion equation with variable coefficients. The method is

Table 20: The value of logarithmic condition number and numerical stability parameters with $\alpha = \beta = 1, \gamma = 0.8$ using relative perturbations $\frac{\|\Delta A\|}{\|A\|} = 10^{-10}$ and $\frac{\|\Delta F\|}{\|F\|} = 10^{-04}$.

n	$\log_{10}(cond(A))$	p_1	p_2
4	4.4506	7.09284×10^{-01}	7.0928×10^{-01}
6	4.8281	2.9594×10^{-01}	2.95943×10^{-01}
8	5.2831	9.76009×10^{-02}	9.75989×10^{-02}
10	5.7974	3.14977×10^{-02}	3.14957×10^{-02}

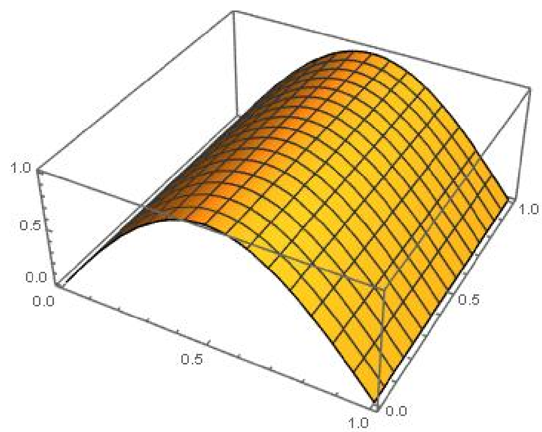

(a) Exact plot.

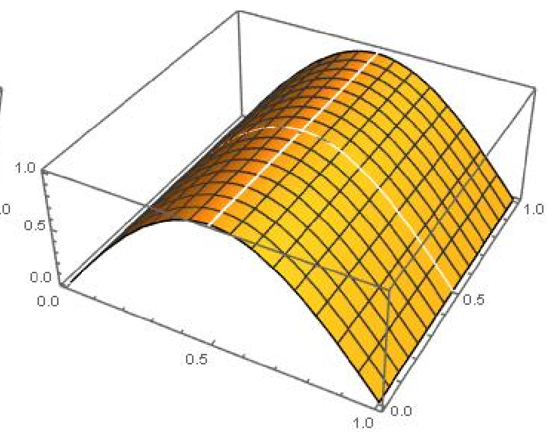

(b) Approximate plot.

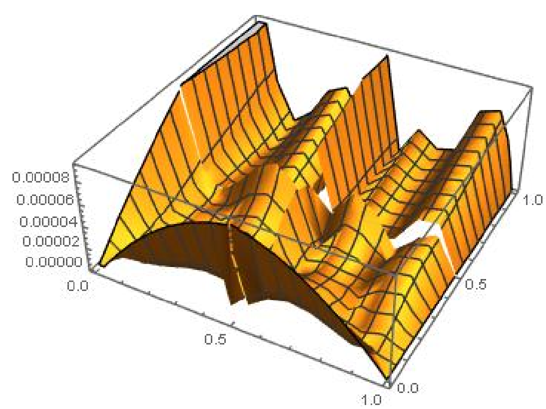

(c) Absolute error plot.

Figure 6: Plot of exact, approximate, and absolute error of Example 6.

adopted because of its several inherent properties, such as continuity, compact support, piecewise-defined functions, representation of polynomials to a certain degree, ability to represent functions at different levels of resolution, and ability to transform the fractional partial differential equations into a system of algebraic equations that can be solved effectively. Furthermore, fractional Chelyshkov wavelet basis functions accurately capture the solution behavior with a relatively small number of basis functions, thereby reducing computational effort. The fractional-order operational matrix for the fractional Chelyshkov wavelet was obtained. The stability analysis is investigated by using perturbation based theory. Convergence and error analyses have also been established. The numerical examples showed that the proposed method yields accurate results for different fractional orders. The error decreases significantly as the wavelet resolution parameters are refined, confirming the method's reliability. A comparison with existing numerical methods is presented, supporting the claim that fractional Chelyshkov wavelets achieve high accuracy. To show the computational efficiency of the proposed method, CPU time and memory usage were reported. Future research may focus on extending the proposed method to nonlinear fractional problems, distributed-order and variable-order fractional models, multidimensional problems, and coupled systems arising from engineering and physical applications.

Funding

This research received no external funding.

Conflicts of Interest

The authors declare no conflicts of interest.

References

[1] Abo-Gabal, H., Zaky, M.A. and Doha, E.H. *Fractional Romanovski–Jacobi tau method for time-fractional partial differential equations with nonsmooth solutions,* Appl. Numer. Math. 182 (2022), 214–234.

[2] Adibmanesha, L. and Rashidinia, J. *Sinc and B-spline scaling functions for time-fractional convection-diffusion equations,* J. King Saud Univ. Sci. 33(2) (2021), 101343.

[3] Chen, Y., Wu, Y., Cui, Y., Wang, Z. and Jin, D. *Wavelet method for a class of fractional convection-diffusion equation with variable coefficients,* J. Comput. Sci. 1(3) (2010), 146–149.

[4] Chui, C.K. *Wavelet analysis and its applications,* Wavelets, 725, 1992.

[5] Faheem, M., Khan, A. and Raza, A. *A high resolution Hermite wavelet technique for solving space–time-fractional partial differential equations,* Math. Comput. Simul. 194 (2022), 588–609.

[6] Inc, M. *The approximate and exact solutions of the space- and time-fractional Burgers equations with initial conditions by variational iteration method,* J. Math. Anal. Appl. 345(1) (2008), 476–484.

[7] Irandoust-Pakchin, S., Dehghan, M., Abdi-Mazraeh, S. and Lakestani, M. *Numerical solution for a class of fractional convection–diffusion equations using the flatlet oblique multiwavelets,* J. Vib. Control 20(6) (2014), 913–924.

[8] Izadkhah, M.M. and Saberi-Nadjafi, J. *Gegenbauer spectral method for time-fractional convection–diffusion equations with variable coefficients,* Math. Methods Appl. Sci. 38(15) (2015), 3183–3194.

[9] Kanna, M.R.R., Kumar, R.P., Nandappa, S. and Cangul, I.N. *On solutions of fractional order telegraph partial differential equation by Crank–Nicholson finite difference method,* Appl. Math. Nonlinear Sci. 5(2) (2020), 85–98.

[10] Kargar, Z. and Saeedi, H. *B-spline wavelet operational method for numerical solution of time-space fractional partial differential equations,* Int. J. Wavelets Multiresolut. Inf. Process. 15(4) (2017), 1750034.

[11] Korkiatsakul, T., Koonprasert, S. and Neamprem, K. *Chebyshev wavelet solutions for time-fractional integro partial differential equation and its application to beam problems,* Compusoft 9(5) (2020), 3677–3684.

[12] Kumbinarasaiah, S. and Mulimani, M. *The Fibonacci wavelets approach for the fractional Rosenau–Hyman equations,* Results Control Optim. 11 (2023), 100221.

[13] Lai, J., Liu, F., Anh, V.V. and Liu, Q. *A space-time finite element method for solving linear Riesz space fractional partial differential equations,* Numer. Algorithms (2021), 1–22.

[14] Luchko, Y. and Gorenflo, R. *An operational method for solving fractional differential equations with the Caputo derivatives,* Acta Math. Vietnam. 24(2) (1999), 207–233.

[15] Md Nasrudin, F.S., Phang, C. and Kanwal, A. *Fractal-fractional advection–diffusion–reaction equations by Ritz approximation approach,* Open Phys. 21(1) (2023), 20220221.

[16] Miller, K.S. *An Introduction to the Fractional Calculus and Fractional Differential Equations*, John Wiley & Sons, 1993.

[17] Ngo, H.T.B., Razzaghi, M. and Vo, T.N. *Fractional-order Chelyshkov wavelet method for solving variable-order fractional differential equations and an application in variable-order fractional relaxation system,* Numer. Algorithms 92(3) (2023), 1571–1588.

[18] Oruç, "O., Esen, A. and Bulut, F. *A Haar wavelet approximation for two-dimensional time fractional reaction–subdiffusion equation,* Eng. Comput. 35(1) (2019), 75–86.

[19] Pariyar, S., Lamichhane, B.P. and Kafle, J. *A time fractional advection–diffusion approach to air pollution: Modeling and analyzing pollutant dispersion dynamics,* Partial Differ. Equ. Appl. Math. 14 (2025), 101149.

[20] Podlubny, I. *Fractional Differential Equations: An Introduction to Fractional Derivatives, Fractional Differential Equations, to Methods of Their Solution and Some of Their Applications*, Elsevier, 1998.

[21] Rahimkhani, P. and Ordokhani, Y. *A numerical scheme based on Bernoulli wavelets and collocation method for solving fractional partial differential equations with Dirichlet boundary conditions,* Numer. Methods Partial Differ. Equ. 35(1) (2019), 34–59.

[22] Rahimkhani, P., Ordokhani, Y. and Lima, P.M. *An improved composite collocation method for distributed-order fractional differential equations based on fractional Chelyshkov wavelets,* Appl. Numer. Math. 145 (2019), 1–27.

[23] Saadatmandi, A. and Dehghan, M. *A tau approach for solution of the space fractional diffusion equation,* Comput. Math. Appl. 62(3) (2011), 1135–1142.

[24] Saadatmandi, A., Dehghan, M. and Azizi, M.-R. *The Sinc–Legendre collocation method for a class of fractional convection–diffusion equations with variable coefficients,* Commun. Nonlinear Sci. Numer. Simul. 17(11) (2012), 4125–4136.

[25] Safdari, H., Rajabzadeh, M. and Khalighi, M. *Solving a nonlinear fractional convection-diffusion equation using local discontinuous Galerkin method,* Appl. Numer. Math. 165 (2021), 22–34.

[26] Saw, V. and Kumar, S. *The Chebyshev collocation method for a class of time fractional convection-diffusion equation with variable coefficients,* Math. Methods Appl. Sci. 44(8) (2021), 6666–6678.

[27] Singh, A., Kanaujiya, A. and Mohapatra, J. *Chelyshkov wavelet method for solving multi-dimensional variable order fractional optimal control problem,* J. Appl. Math. Comput. 70 (2024), 3135–3160.

[28] Singh, A., Kanaujiya, A. and Mohapatra, J. *Euler wavelets method for optimal control problems of fractional integro-differential equations,* J. Comput. Appl. Math. 454 (2025), 116178.

[29] Singh, A., Kanaujiya, A. and Mohapatra, J. *Fractional Legendre wavelet approach resolving multi-scale optimal control problems involving Caputo–Fabrizio derivative,* Numer. Algorithms 99 (2025), 101–132.

[30] Singh, A., Kanaujiya, A. and Mohapatra, J. *Fractional-order Euler wavelet technique for multidimensional distributed-order optimal control problem,* Commun. Nonlinear Sci. Numer. Simul. 152 (2025), 109316.

[31] Singh, A., Kanaujiya, A. and Mohapatra, J. *Wavelet technique for variable-order modified Caputo–Fabrizio optimal control problems,* Iran J. Sci. 50 (2026), 797–811.

[32] Singh, A., Kanaujiya, A. and Mohapatra, J. *An efficient generalized Lucas wavelet operational matrix method for optimal control problems,* J. Comput. Appl. Math. 471 (2026), 116749.

[33] Singh, A., Kanaujiya, A. and Mohapatra, J. *Fractional order Chelyshkov wavelet method for variable-order time delay optimal control problem,* J. Comput. Appl. Math. 486 (2026), 117703.

[34] Tsuchiya, T. and Kumagai, A. *Numerical simulation of acoustic imaging using a combination of finite difference time domain and boundary integral equation methods,* Jpn. J. Appl. Phys. 48(7S) (2009), 07GN02.

[35] Uddin, M. and Haq, S. *RBFs approximation method for time fractional partial differential equations,* Commun. Nonlinear Sci. Numer. Simul. 16(11) (2011), 4208–4214.

[36] Wang, Y. and Zhu, L. *Solving nonlinear Volterra integro-differential equations of fractional order by using Euler wavelet method,* Adv. Differ. Equ. (2017), 1–16.

[37] Xu, X. and Xu, D. *Legendre wavelets direct method for the numerical solution of time-fractional order telegraph equations,* Mediterr. J. Math. 15 (2018), 1–33.

[38] Yadav, P., Jahan, S. and Nisar, K.S. *Fibonacci wavelet method for time fractional convection–diffusion equations,* Math. Methods Appl. Sci. 47(4) (2024), 2639–2655.

[39] Yousefi, S.A. and Dehghan, M. *The use of He's variational iteration method for solving variational problems,* Int. J. Comput. Math. 87(6) (2010), 1299–1314.

[40] Zada, L. and Aziz, I. *Numerical solution of fractional partial differential equations via Haar wavelet,* Numer. Methods Partial Differ. Equ. 38(2) (2022), 222–242.

[41] Zhou, F. and Xu, X. *The third kind Chebyshev wavelets collocation method for solving the time-fractional convection diffusion equations with variable coefficients,* Appl. Math. Comput. 280 (2016), 11–29.